AN ABSTRACT OF THE THESIS OF

Christopher P. Scott for the degree of Master of Ocean Engineering in Ocean Engineering presented on February 25, 2005.

Title: Large-Scale Laboratory Observations of Wave Breaking Turbulence on a Fixed Barred Beach

Abstract approved:

Redacted for Privacy

Daniel T. Cox

This thesis presents the details of a large-scale laboratory experiment to study the turbulence generated by waves breaking on a fixed barred beach. The data set includes comprehensive measurements of free surface displacement and fluid velocity for one random and one regular wave case.

Observations of the time-averaged turbulent kinetic energy per unit mass, $\overline{k}$, show that the turbulence generated by wave breaking was greatest at the bar crest and did not fully dissipate prior to reaching the bed. This indicates that, even in a time-averaged sense, wave breaking turbulence may be important for near-bed processes on a barred beach. Onshore of the bar, turbulence was generally confined to the upper part of the water column and dissipated once the waves reformed (approximately 1.5 wavelengths onshore of the bar crest). The turbulent structure was the same in the random and regular wave cases; however, the magnitude of $\overline{k}$ was much less in the random wave case, despite similar offshore wave conditions.

Three methods were used to separate the wave-induced and turbulent components of velocity: ensemble averaging, high-pass filtering, and a differencing method proposed by Trowbridge (1998). The magnitude of $\overline{k}$ varied by as much as a factor of 5 among these methods, but qualitatively, the cross-shore and vertical structure was independent of the method used. The differencing method agreed closely with ensemble averaging in terms of the magnitude and structure of time-averaged quantities and in the signature of the time-dependent turbulent kinetic energy. Given this agreement and the general acceptance of ensemble averaging as an appropriate method to separate wave-induced and turbulent components of velocity for regular waves (Svendsen 1987), the differencing method appears to be the most suitable for application to random waves, such as those observed in the field.

Large-Scale Laboratory Observations of Wave Breaking Turbulence on a Fixed Barred Beach

by
Christopher P. Scott

A THESIS

submitted to

Oregon State University

in partial fulfillment of
the requirements for the
degree of

Master of Ocean Engineering

Presented February 25, 2005
Commencement June 2005

Master of Ocean Engineering thesis of Christopher P. Scott presented on February 25, 2005.

APPROVED:

Redacted for Privacy

Major Professor, representing Ocean Engineering

Redacted for Privacy

Head of the Department of Civil, Construction, and Environmental Engineering

Redacted for Privacy

Dean of the Graduate School

I understand that my thesis will become part of the permanent collection of Oregon State University libraries. My signature below authorizes release of my thesis to any reader upon request.

Redacted for Privacy

Christopher P. Scott, Author

ACKNOWLEDGEMENTS

This work was partially funded by the National Science Foundation under grants No. CMS-0086571, EEC-0244205 and OCE-0351741.

In addition to the opportunity to study at OSU, I am thankful for the direction and encouragement from my advisor, Daniel Cox. I am also thankful that Terry Dibble remained "semi-retired" and sacrificed so many sunny biking days to patiently teach me about the lab. I am grateful for the patience, guidance, laughter, and food given to me by Tim Maddux. Joseph Long's hard work made this experiment possible and I am indebted to him for his honest friendship. The helpful questions and encouragement from my committee members, Merrick Haller and Tuba Özkan-Haller, are much appreciated. I must also thank all of the students who were a part of this project, including: Jason Killian, Patricio Catalan, and Jason Magalen for surveying the beach, Dan Clark for metal fabrication, and Emi Fujii, Sungwon Shin, and Neil Clayton for their work in setting up and collecting the data. I would also like to thank Takayuki Suzuki and Nobuhito Mori for their tour of Japan and contribution to this work.

Finally, I would like to thank my Heavenly Father, family, and friends for their love, gifts of encouragement, and prayer that have been a blessing to me throughout my time here. My hope is that everyone knows how grateful I am.

CONTRIBUTION OF AUTHORS

Tim Maddux provided direction in every stage of this experiment, including the design and installation of the model beach, ADV operation, data collection, analysis, and scientific interpretation. Joseph Long worked on the construction of the model beach, experimental setup, data collection, and analysis.

TABLE OF CONTENTS

TABLE OF CONTENTS (Continued)

LIST OF FIGURES

LIST OF TABLES

LIST OF APPENDICIES

LIST OF APPENDICIES (Continued)

LIST OF APPENDIX FIGURES

LIST OF APPENDIX FIGURES (Continued)

LIST OF APPENDIX FIGURES (Continued)

LIST OF APPENDIX FIGURES (Continued)

LIST OF APPENDIX TABLES

Large-Scale Laboratory Observations of Wave Breaking Turbulence on a Fixed Barred Beach

1. General Introduction

The coastal zone is a densely populated region vital to trade, tourism, and recreation. Our attraction to the coast is reflected in the fact that more than half of the U.S. population currently lives within 50 miles of the coastline and the population density in coastal regions is 2-3 times larger than in the nation as a whole (U.S. Commission on Ocean Policy 2004). This is also a highly dynamic region where large changes in the shoreline can occur over timescales ranging from hours to years. To use the coastal zone effectively, coastal managers must possess tools to accurately predict how the shoreline will change. However, the development of these tools has been limited by our understanding of the processes governing sediment transport and the difficulty in obtaining detailed measurements of nearshore processes within this region.

One process important to sediment transport is wave breaking within the surf zone, where organized wave energy is converted to turbulence which can initiate sediment suspension or keep particles in suspension (Fredsøe and Deigaard 1992). At the surface of the ocean, the magnitude of this turbulent energy is much larger than the turbulence generated in the boundary layer near the seabed. However, wave breaking turbulence decays as it is transported to the bottom and the degree to which it contributes to the near-bed turbulent energy is unclear. To accurately predict sediment

transport the distribution of turbulence generated by wave breaking and the bottom boundary layer must be known.

Experiments aimed at understanding wave breaking turbulence have been conducted in small- and large-scale laboratory flumes as well as the field. The data obtained in these experiments have formed our understanding of turbulence in the nearshore and are briefly summarized in the following section.

1.1 Literature Review

1.1.1 Small-Scale Laboratory Experiments

The majority of experimental work that has formed the foundation of our understanding of wave breaking turbulence was conducted in small-scale, long (or "two-dimensional") wave flumes. These flumes were typically on the order of 50 m long, 1 m wide, and 1 m deep with a planar beach at one end to initiate breaking (slopes ranging from 1:20 – 1:40). Regular waves were used in these tests with wave heights ranging from 10 cm < H_0 < 22 cm, and periods from 0.9 s < T < 5.0 s. Glass sidewalls allowed the use of laser-Doppler-velocimeters (LDV) to measure the flow field and video/photographic techniques to visualize the characteristic features of the flow.

Stive (1980) conducted one of the first experiments specifically designed to study the internal flow field of breaking waves in the inner surf zone. In this experiment, Stive (1980) measured the velocity and pressure fields under spilling breakers and showed that the quasi-steady breaking wave model proposed by Peregrine and Svendsen (1978) qualitatively agreed with the observed periodic and turbulent velocities in the inner surf zone. This model essentially consists of a turbulent mixing region at the face of the broken wave (i.e. a "roller" or "bore") that spreads and decays into a wake region behind the crest.

Two-years later, Nadaoka and Kondoh (1982) identified several key features of the flow field in a detailed study of spilling and plunging breakers. The flow field was separated into two zones in the cross-shore direction: a transition zone near the onset of breaking, and the bore-establishment zone, also referred to as the inner surf zone. In the inner surf zone, the flow consisted of an upper layer and a bottom layer. In the upper layer, visual observations revealed the presence of large-scale eddies, small-scale turbulence, and entrained air. In the bottom layer, LDV measurements revealed small-scale turbulence that originated in the upper layer along with small-scale turbulence generated in the bottom boundary layer. Large turbulent velocities were observed 5 mm above the bottom that were not characteristic of boundary layer turbulence (turbulence in the boundary layer should be correlated with the wave phase or an increase in the near bottom wave velocity). This observation indicated that the turbulence from wave breaking reached the bed.

Svendsen (1987) utilized the turbulent velocities obtained from the previous two experiments along with additional measurements by Stive and Wind (1982) and Hattori and Aono (1985) to investigate the time-averaged structure and temporal variation of the turbulent kinetic energy due to waves breaking on a plane slope. In every case the time-averaged turbulent kinetic energy showed little vertical variation and was large near the bottom. This supported the idea that large-scale vortices generated by wave breaking create intense mixing that transports turbulence from the surface to the bed. Additionally, the temporal variation of turbulent kinetic energy was small in Stive and Wind's (1982) tests, indicating that time-averaged quantities are appropriate for describing the turbulence under breaking waves. Svendsen (1987) also reviewed the three different methods used in these experiments to separate the wave-induced and turbulent components of velocity (ensemble averaging, correlation with the free surface, and high-pass filtering). He concluded that ensemble averaging was the most suitable (or only) method when considering regular waves, but could not be extended to random waves in the field, which was a problem with no clear solution.

Nadaoka *et al.* (1989) conducted a second experiment to investigate the structure of the large-scale vortices, or eddies, observed by Nadaoka and Kondoh (1982). Using flow visualization techniques, Nadaoka *et al.* (1989) concluded that the large-scale eddies produced by wave breaking were one of the most important features in the surf zone due to the intense turbulence and vorticity produced by them. These eddies were two-dimensional and horizontal around the wave crest (axis of rotation parallel to the

crest), and transformed into three-dimensional, obliquely descending eddies behind the wave (axis of rotation approximately 45° to the direction of wave propagation). These eddies created large Reynolds stresses in the upper water column, and observations showed that they transported tracer particles all the way to the bed. This confirmed that wave breaking turbulence, and specifically the large-scale eddies generated by wave breaking, may act as a mechanism for the suspension of sand.

Ting and Kirby (1994) also observed large-scale eddies while investigating differences in the undertow and turbulence generated by spilling and plunging breakers. They found fundamental differences in the flow fields associated with these breaker types, despite similar deep water wave conditions. In the spilling case, the undertow and turbulent intensity showed a strong dependence on depth, but very little variation with wave phase. Whereas, in the plunging case, the undertow and turbulent intensity were virtually uniform with depth and large turbulent intensities were highly correlated with the passage of the wave crest. This resulted in a net offshore transport of turbulence by the mean flow (including the orbital wave motion) in the spilling wave case and a net onshore transport of turbulence by the mean flow in the plunging wave case. Ting and Kirby (1994) suggested that the transport of turbulence can be correlated to the transport of sediment; therefore, the spilling wave case would correspond to an eroding beach and the plunging wave case would correspond to an accreting beach.

Cox *et al.* (1994 and 1996) collected detailed observations of the turbulence within the boundary layer and in the upper water column in the presence of spilling waves on a roughened slope. They showed that offshore, turbulence was confined to the boundary layer, whereas in the inner surf zone, the turbulence generated by wave breaking spread and decayed downward, which was consistent with what had been observed in previous experiments. Cox and Kobayashi (2000) identified intermittent and coherent events caused by large-scale eddies that spread into the boundary layer in the surf zone. The turbulent energy contained in these eddies was an order of magnitude larger than the turbulence generated locally within the boundary layer, indicating that they may be important for the suspension of sediments, as suggested by Nadaoka *et al.* (1989).

1.1.2 Large-Scale Laboratory Experiments

Despite the attention that wave breaking turbulence received in small-scale flumes, large-scale research on wave breaking turbulence has been limited. It should be noted that although there is an absence of large-scale laboratory data focusing specifically on wave breaking turbulence, large-scale wave flumes have been used to study other nearshore processes, including cross-shore beach profile change. These tests are summarized by Dette *et al.* (2002) and are omitted here since they do not directly address wave breaking turbulence. Sancho *et al.* (2001) conducted the SPANWAVE-SPPORITA experiment in the Canal de Investigación y Experimentación Maritima (CIEM wave flume) at the Polytechnic University of Catalonia in Barcelona, Spain.

Their objectives were to obtain detailed large-scale measurements of the turbulence and mean flow present over a fixed barred beach using regular and random waves. The model beach was constructed of non-smoothed concrete and designed to approximate an equilibrium bar based on observations from Duck, NC and the SUPERTANK experiment (Kraus *et al.* 1992). Measurements of the free-surface elevation, pressure, and water particle velocity were collected. Thus far, only the experimental setup (Sancho *et al.* 2001) and characteristics of the mean flow (Tomasicchio and Sancho 2002) have been presented; therefore, no conclusions can be made regarding the turbulence generated by wave breaking.

1.1.3 Field Experiments

In addition to the small- and large-scale laboratory tests, field experiments have been conducted to observe the turbulence generated in the surf zone. George *et al.* (1994) used hotfilm anemometry to estimate the turbulent dissipation rate (ε) and turbulence intensity (u') from spilling and plunging random waves at Scripps Beach in La Jolla, CA. Turbulence from wave breaking was largest at the surface and decayed slowly toward the bottom, consistent with the strong vertical mixing observed in the laboratory. However, the magnitude of the Froude scaled turbulence intensity $\left(u'/\sqrt{gh}\right)$ was as much as a factor of 4 smaller than the laboratory results of Stive (1980) who used monochromatic waves and a different technique to extract the turbulent signal.

Trowbridge and Elgar (2001) analyzed the balance of turbulent dissipation with shear production and the depth-averaged wave energy dissipation over a sandy beach in Duck, NC. They estimated that shear production balanced dissipation, but both were 2 orders of magnitude less than the depth-averaged energy loss in the wave field. This indicated that wave breaking turbulence did not influence the turbulent energy at the measurement location, which was 1 m above the bottom in approximately 4.5 m of water. This may have been due to the fact that the field observations were in the outer surf zone, whereas wave breaking turbulence was most influential in the inner surf zone of the laboratory.

1.2 Summary

Small-scale laboratory experiments have established the importance of wave breaking to the production of large-scale eddies and turbulence within the surf zone, which may act as a mechanism for sediment suspension. Field tests have qualitatively confirmed these observations; however, they lack the high spatial resolution and simplified forcing necessary to make a direct comparison. Large-scale laboratory experiments focused on the turbulence generated by wave breaking can be used to confirm the observations from small-scale tests, but are virtually non-existent.

In light of this, the experiment discussed in this thesis was conducted to provide a synoptic picture of the turbulence generated by random and regular waves breaking over a fixed barred beach at prototype scale. It is written in the manuscript format and

organized as follows: Section 2 includes the manuscript, which discusses the details of the experiment, a comparison of three methods to separate the wave-induced and turbulent components of velocity, and observations of the time-averaged turbulent kinetic energy over the bar. Section 3 provides a summary of the major conclusions. Additional information that could not be included in the manuscript due to page limitations is included in Appendices A – G and noted within Section 2 using brackets (e.g., [Refer to Appendix A.1 for ...]). Appendix A contains additional information on the experimental setup and wave conditions. Appendix B provides further detail on the repeatability of the wave conditions and post-processing of the velocity time series. Example applications of the methods used to extract the turbulent signal from the total velocity are shown in Appendix C. The alongshore variation of turbulence estimates over the bar are given in Appendix D. Appendix E describes a preliminary analysis of the correlation between wave breaking and changes in the mean flow. Appendices F and G contain presentations of this research from the 29th International Conference on Coastal Engineering held in Lisbon, Portugal, and the Oceans/Techno-Ocean'04 conference held in Kobe, Japan in November, 2004, respectively.

2. Large-Scale Laboratory Observations of Turbulence on a Fixed Barred Beach

Christopher P. Scott

Daniel T. Cox

Timothy B. Maddux

Joseph W. Long

O.H. Hinsdale Wave Research Laboratory

Oregon State University, Corvallis, OR 97331-2302, USA

Submitted to:

Measurement Science and Technology: Special Issue on Water Wave Measurements

Institute of Physics Publishing, Inc

The Public Ledger Building, Suite 929

150 South Independence Mall West

Philadelphia, PA 19106, USA

2.1 Abstract

The details of a large-scale laboratory experiment to study the turbulence generated by waves breaking on a fixed barred beach are presented. The data set includes comprehensive measurements of free surface displacement and fluid velocity for one random and one regular wave case. Observations of the time-averaged turbulent kinetic energy per unit mass, $\overline{k}$, show that the turbulence generated by wave breaking was greatest at the bar crest and did not fully dissipate prior to reaching the bed. This indicates that, even in a time-averaged sense, wave breaking turbulence may be important for near-bed processes. Onshore of the bar, turbulence was generally confined to the upper part of the water column and had dissipated once the waves reformed (approximately 1.5 wavelengths onshore of the bar crest). The turbulent structure was the same in the random and regular wave cases; however, the magnitude of $\overline{k}$ was much less in the random wave case, despite similar offshore wave conditions. Additionally, three methods were used to separate the wave-induced and turbulent components of velocity: ensemble averaging, high-pass filtering, and a differencing method proposed by Trowbridge (1998). The magnitude of $\overline{k}$ varied by as much as a factor of 5 among these methods, but qualitatively, the cross-shore and vertical structure was independent of the method used. The differencing method agreed closely with ensemble averaging in terms of the magnitude and structure of time-averaged quantities, and in the signature of the time-dependent turbulent kinetic energy. Given this agreement, the differencing method appears to be the most suitable for application to random waves, such as those observed in the field.

2.2 Introduction

In the surf zone, wave energy is transformed into turbulent energy through breaking. The turbulence generated by wave breaking can dominate surf zone flows (Trowbridge and Elgar 2001) and processes of sediment suspension (Fredsøe and Deigaard 1992). Furthermore, the difficulty in making direct observations of surf zone turbulence has hindered our ability to adequately quantify and predict sediment transport. Prototype-scale laboratory experiments have been suggested as a facilitator for improved understanding of the processes of breaking waves and their associated turbulence (Thornton *et al.* 2000).

Prototype-scale laboratory experiments are necessary because many of the existing studies on wave breaking turbulence have been conducted in small-scale laboratory flumes (e.g., Stive 1980, Nadaoka and Kondoh 1982, Ting and Kirby 1994, Cox *et al.* 1995) and scaling issues may arise when extrapolating hydrodynamic quantities, such as the vertical variation of horizontal turbulence intensity, to field conditions. Additionally, most of these experiments were conducted using planar beaches, and only recently has attention been given to complex bathymetries such as a barred beach (e.g., Sancho *et al.* 2001), despite the numerous modeling efforts for predicting field-observed bar motions (e.g., Hoefel and Elgar 2003). In the laboratory, repeatable wave conditions and the use of a fixed bed provides a unique opportunity to collect a detailed, synoptic data set without the influence of three-dimensional wave and current

fields, tides, and wind. It also allows the use of sensitive instrumentation likely to be damaged in a field deployment.

The objective of this experiment is to provide a large-scale, synoptic picture of the time-averaged turbulent kinetic energy in the nearshore, and to determine whether the turbulence from wave breaking is transported to the bed on a barred profile. Additionally, we compare three methods to separate turbulent and wave-induced fluid velocity components to determine whether the method used affects the magnitude or spatial structure of the turbulence estimates. Section 2.3 briefly describes these three methods, followed by the experimental setup and post-processing of the data in Sections 2.4 and 2.5, respectively. Section 2.6 outlines the application of each method to the data and Section 2.7 compares the turbulence estimates from all three. Observations of the cross-shore and vertical structure of the turbulence generated over the bar are presented in Section 2.8, followed by the main conclusions in Section 2.9.

2.3 Methods to Separate Wave and Turbulent Motions

In the nearshore, the observed fluid velocity (u) can be decomposed into mean, wave-induced, and turbulent components as follows:

$$u = \overline{u} + \tilde{u} + u' \tag{2.1}$$

where an overbar denotes time-averaged (mean) quantities, a tilde denotes wave-induced quantities, and a prime denotes turbulent quantities. Separating the wave-induced and turbulent components is difficult and several methods are suggested in the

literature. Svendsen (1987) reviewed three of these methods and compared scaled measurements of the time-averaged turbulent kinetic energy per unit mass $(\bar{k})$ obtained from the laboratory experiments of Stive and Wind (1982), Nadaoka and Kondoh (1982), and Hattori and Aono (1985), where $\bar{k}$ is defined as:

$$\bar{k} = \frac{1}{2}\left(\overline{u'u'} + \overline{v'v'} + \overline{w'w'}\right) \tag{2.2}$$

where u, v, and w are the cross-shore, alongshore, and vertical velocities, respectively. Despite the different methods used to separate the turbulent signal, Svendsen (1987) observed that characteristic features, such as a weak variation of $\bar{k}$ over depth, were consistent for all of the measurements when scaled using the squared shallow water wave speed. In this work, three separation methods were applied to the two data sets collected. This allowed for a direct comparison of the turbulent quantities and eliminated errors that may arise when scaling the results obtained from different experiments. In addition to comparing two of the methods reviewed by Svendsen (1987), ensemble averaging and high-pass filtering, we added a third technique proposed by Trowbridge (1998).

2.3.1 Ensemble Averaging

When regular waves are studied, the wave-induced velocity can be estimated by averaging the same point in the wave phase over many successive waves (ensemble averaging) and the turbulent component can then be estimated using Eq. 2.1. This method has been used extensively in the literature (e.g., Stive and Wind 1982, Ting

and Kirby 1994, and Cox *et al.* 1995) and Svendsen (1987) concluded that it must be considered the only well-defined way of separating wave and turbulent motions when discussing regular waves. It also has the advantage of allowing large, low-frequency vortices, typically neglected by other methods, to be recorded as turbulence, provided they are not identically repeated wave to wave. An obvious limitation of this method is that it cannot be applied to truly random waves in the field. However, in the laboratory this method can be applied to random waves by collecting many realizations of the same velocity time series at a single location and averaging these realizations to obtain the wave-induced velocity.

2.3.2 High-Pass Filtering

When waves are not repeatable, high-pass filtering can be used to separate the wave-induced and turbulent components of velocity by specifying a cutoff frequency separating the wave and turbulent timescales, then applying standard filtering techniques to isolate the high-frequency (turbulent) component. Choosing an appropriate cutoff frequency can be difficult, and it is possible that a single cutoff separating these scales is physically unattainable (Nadaoka *et al.* 1989). Depending on the cutoff frequency chosen, this method may neglect large-scale vortices produced by breaking that are of a lower-frequency than the higher harmonics of the organized wave motion. In fact, Svendsen (1987) observed that scaled turbulence estimates obtained using the high-pass filtering method were generally smaller than those obtained using ensemble averaging.

2.3.3 Differencing

Trowbridge (1998) proposed a technique that utilizes the difference between the measured velocities (Δu) from two closely spaced sensors to estimate the average turbulent velocity variance and covariance between the sensors. For example, the turbulent velocity variance in the cross-shore direction $\left(\overline{u'u'}\right)$ can be estimated as follows:

$$\left\langle \overline{u'u'} \right\rangle = \frac{1}{2}\mathrm{var}(\Delta u) \tag{2.3}$$

where $\langle\ \rangle$ is used to note a spatial average between the sensors, u is the total velocity, and $\Delta u = u_1 - u_2$, where u_1 and u_2 are the observed total velocity from each of the two sensors. This method can be applied to random waves and requires that the sensors be separated such that the wave component of velocity is correlated and the turbulent component is uncorrelated between the two sensors. In general terms, this means that the separation distance between the sensors must be slightly larger than the largest eddy produced by wave breaking. In addition, this separation should be perpendicular to the direction of wave propagation (i.e. parallel to the wave crests), which causes errors when the seas are multidirectional.

2.4 Experimental Setup

2.4.1 Large Wave Flume and Barred Profile

The experiment was conducted in the large wave flume at Oregon State University's O.H. Hinsdale Wave Research Laboratory. The basin is 104 m long, 3.7 m wide, and 4.6 m deep with a programmable flap-type wavemaker equipped with active wave absorption and maximum wave capability of $H = 1.6$ m at $T = 3.5$ s. For this project, a model beach was constructed by fixing concrete slabs to the sidewalls of the flume, resulting in the piecewise continuous profile shown in Figure 2.1c. The model bathymetry approximated the bar geometry for the average profile observed on October 11, 1994, of the DUCK94 field experiment (e.g., Garcez Faria *et al.* 2000) at a 1:3 scale. The model was compressed in the cross-shore relative to field-observed bars due to the limitation of the flume length. Nevertheless, it captured the hydrodynamic processes of wave breaking and reforming common to natural barred beaches. The friction factor, f_w, was estimated using the semitheoretical expression developed by Jonsson (1966) for rough turbulent flow:

$$\frac{1}{4\sqrt{f_w}} + \log\left(\frac{1}{4\sqrt{f_w}}\right) = \log\left(\frac{A_b}{k_s}\right) - 0.08 \qquad (2.4)$$

where A_b is the excursion amplitude at the bed estimated using linear wave theory and k_s is the Nikuradse sand roughness typically estimated using the grain diameter $(k_s = 2d_{50})$. Using an estimate range of $0.04 \text{ mm} < k_s < 0.2$ mm and the breaking wave heights and periods listed in Table 2.1 in a water depth of 0.80 m, estimates of the wave friction factor fell in the range of $0.005 < f_w < 0.007$. In comparison,

applying the same approach to the average wave conditions from the 8-meter array on October 11, 1994, at Duck, NC (H_{mo} = 1.8 m, T_p = 6.6 s, h=8.3 m) with d_{50} = 0.2 mm yielded a friction factor of f_w = 0.008. [Refer to Appendix A.1 for additional information on the model beach construction.]

2.4.2 Wave Conditions and Free Surface Measurements

In this study, a random time series approximating a narrow banded sea (TMA spectrum, $\gamma = 20$) was used to study the wave breaking process under forcing similar to the field. Regular waves were also used to allow the ensemble averaging technique to be applied. In both cases, the target offshore wave height and period were scaled using the average significant wave height (H_{mo} = 1.8 m) and peak period (T_p = 6.6 s) observed at the 8-meter array on October 11, 1994, of the DUCK94 field experiment. Active wave absorption was used for the regular wave case. It was not used for the random wave case because it limited the size of the waves that could be generated. Additionally, preliminary investigations using similar wave conditions and the underlying 1:36 planar beach indicated that active wave absorption did not significantly reduce energy at low frequencies for the random wave case.

Resistance-type wave gages sampling at 50 Hz were used to measure the free surface elevation (η) at 28 locations in the basin. To validate the repeatability of the experiment, 6 gages remained fixed during the study (x = 23.45 m, 45.40 m, 52.73 m, 60.04 m, 70.99 m, 81.97 m) and one was mounted on the wavemaker (x = 0.00 m).

Additionally, η was measured using three wave gages mounted on a movable cart used for collecting velocity profiles, as shown in Figure 2.2.

The deep water and breaking wave characteristics for the random and regular cases are listed in Table 2.1.

Table 2.1. Deep water and breaking wave conditions measured during the experiment.

	T [s]	H_0 [m]	L_0 [m]	H_b [m]	L_b [m]	ξ_b [-]	t_{dur} [min]	N_{waves} [-]
Random	4.0	0.59	25.0	0.64	10.9	0.35	20	342
Regular	4.0	0.64	25.0	0.75	10.9	0.32	10	150

The subscripts $(\,)_0$ and $(\,)_b$ are used to denote deep water and breaking parameters, respectively. For the random wave case, T is the spectral peak period and H is the significant wave height calculated using zero-upcrossing. For the regular wave case T and H are the ensemble averaged wave period and wave height calculated using zero-upcrossing. In both cases the deep water wave length (L_0) and wave height (H_0) were calculated using linear wave theory. The average slope on the offshore side of the bar $(\tan\alpha_b = 1/18)$ was used to calculate the Iribarren number $\left(\xi_b = \dfrac{\tan\alpha_b}{\sqrt{H_b/L_0}}\right)$. It is noted that the values obtained for ξ_b are slightly below the plunging criterion $0.4 < \xi_b < 2.0$ suggested by Battjes (1974). However, the random waves were observed to be both plunging and spilling as far offshore as $x = 42$ m, and the regular waves were plunging at $x = 53$ m. Approximately $N = 342$ waves were recorded in the

random wave case, which exceeds the minimum of 200 prescribed by Goda (2000) for a repeatable sea state. For the regular wave case, $N = 150$ waves were used, exceeding the number used in previous studies (e.g., Ting and Kirby 1994: $N \cong 100$, Cox *et al.* 1995: $N = 50$).

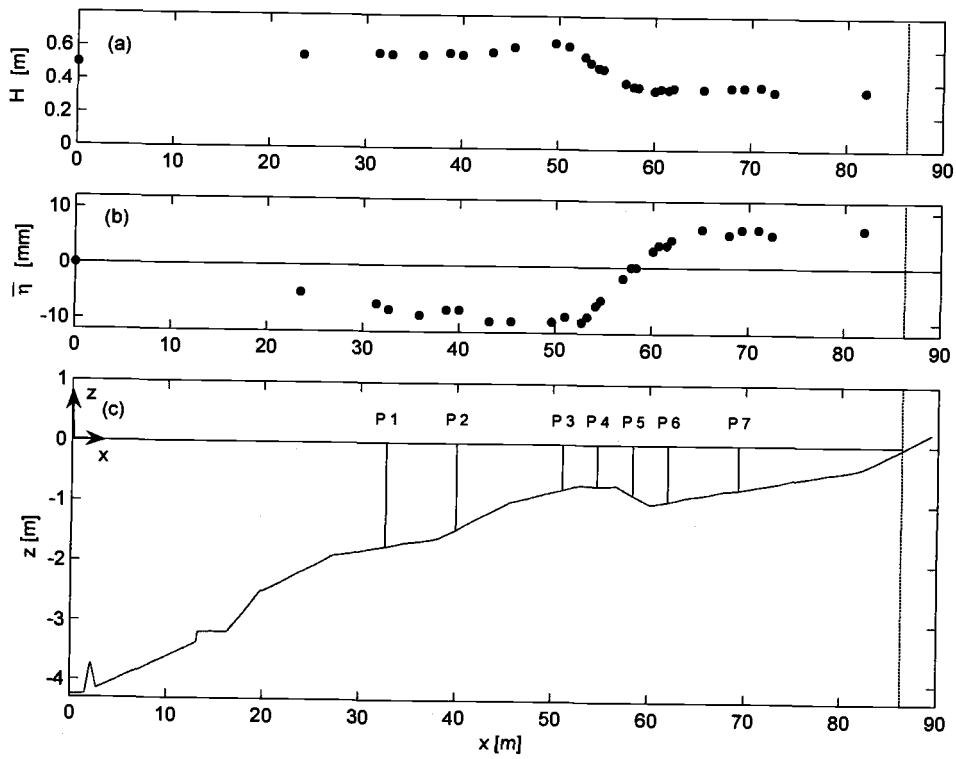

Figure 2.1. Cross shore variation of H (a) and $\overline{\eta}$ (b) for the random wave case. Surveyed bathymetry and locations of velocity profiles P1-P7 (c). Wavemaker located at $x = 0$, still water shoreline indicated by (--).

Figures 2.1a and 2.1b show the cross-shore variation of H and mean water level $(\overline{\eta})$ for the random wave case, clearly showing the shoaling ($x < 50$ m), breaking (50 m $< x <$ 60 m), and reforming ($x > 60$ m) regions. The measured variation in $\overline{\eta}$

was consistent with Bowen *et al.* (1968) who found that the maximum set-down occurs slightly onshore of breaking. [The cross-shore variation of H and $\overline{\eta}$ for the regular wave case is shown in Appendix A.2.]

2.4.3 Velocity Measurements

Vertical profiles of velocity time series were recorded at seven cross-shore locations (P1-P7, Figure 2.1c). Of primary interest were the profiles at the bar crest (P4), where wave breaking was most intense, and just onshore of the crest where wave breaking turbulence was carried onshore (P5 and P6). At each of the 7 cross-shore locations, time series were recorded at 8 vertical locations: 1 cm, 5 cm, and 10 cm above the fixed bed, followed by 5 additional elevations evenly-spaced between 10 cm above the bed and trough level.

At each vertical location, velocities were sampled synchronously at 50 Hz using three 3D, down-looking SonTek 16 MHz Micro Acoustic Doppler Velocimeters (ADVs). The ADVs were collocated in the vertical and cross-shore, but separated in the alongshore (Figure 2.2). The alongshore separation was designed to test whether each ADV observed the same wave-induced component of velocity when applying the differencing method. For the random waves, the spacing between the ADVs was 26 cm and 60 cm with the outermost ADVs 137 cm and 142 cm from the sidewalls. This allowed for as large a separation scale as possible while minimizing the effect of the sidewalls on the observed velocities. For the regular wave case, only two ADVs

were used (A500 and A507) with a 60 cm alongshore spacing. The coordinate system, shown in Figures 2.1c and 2.2, was x positive onshore, z positive up, and y consistent with a right-hand coordinate system. The origin was located at the intersection of the wavemaker and the still water line. [Refer to Appendix A.1 for photographs of the instrument cart.]

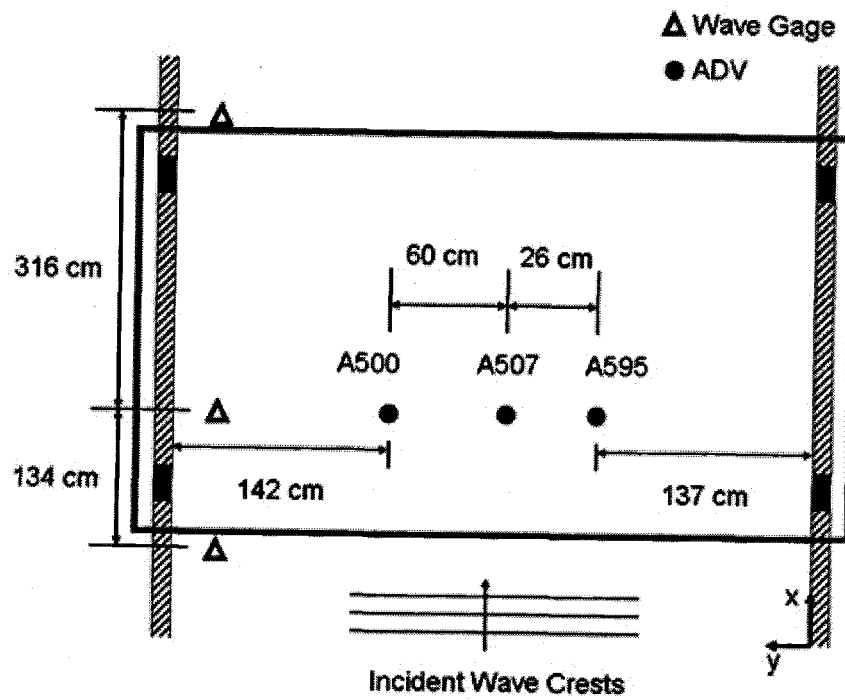

Figure 2.2. Plan view of the movable instrument cart with the locations of the ADV array and three wave gages shown. All three ADVs were collocated in the vertical and cross-shore directions.

To obtain a synoptic data set, the same 20 minute random time series was run at each of the 8 elevations for all 7 profiles (56 total runs), and each run was synchronized to the start of wavemaker motion. Data for the regular wave case were collected in 60 minute runs, during which time the velocity was measured at 4 elevations in the profile by recording at each elevation for 10 minutes. The first 5 minutes of each

60 minute run were eliminated to allow the wave conditions to reach a steady state. The still water interval between each run was 20 minutes for both random and regular waves.

2.5 Data Reduction

2.5.1 Free Surface

All free surface data were reduced using ensemble averaging techniques. For the random wave case, this consisted of averaging 56 realizations of the 20 minute time series for each of the 7 fixed wave gages, and 8 realizations for the three wave gages on the movable cart with the ADV array. For the regular wave case, approximately 8400 waves were averaged for each of the fixed wave gages, and 1200 waves were averaged for the gages on the cart. Seaward of breaking, the average standard deviation of the ensemble averaged wave was less than 1.0 cm (1.5 % of full scale) and 1.5 cm (2.4% of full scale) for the random and regular wave cases, respectively, verifying the repeatability of the wave conditions. [Figures illustrating this repeatability are included in Appendix B.1.]

2.5.2 Velocity

All velocity time series were post-processed to address three sources of noise: signal dropouts and spikes, Doppler noise, and instrument vibration. Signal dropouts due to instruments coming out of the water, and signal spikes caused by air bubbles or a lack

of particulate matter within the flow are common when using ADVs in the surf zone (e.g., Elgar *et al.* 2001). In this test, valid measurements were defined as those having a signal-to-noise ratio (SNR) greater than 10 dB and correlation greater than 70%, where these quantities are the average value along all three ADV beams. Additionally, the phase-space-threshold criterion outlined by Goring and Nikora (2002) was used to identify spikes that were not identified by the SNR and correlation thresholds. After invalid samples were identified, a cubic spline between valid samples was used to replace them. The median percentage of the record identified as invalid was 2.3% and 2.7% for the random and regular wave cases, respectively, with significantly higher values (20-30%) near trough level at P4 and P5. Figure 2.3 shows the raw and despiked cross-shore velocity spectra for ADV A500 at P4, 34 cm above the bed. The -5/3 slope, characteristic of an inertial subrange, is biased high in the raw data at frequencies above 2-3 Hz. This is indicative of white noise in the data, and the energy associated with that high-frequency portion of the spectrum is typically referred to as the noise floor. It is clear that after removing signal dropouts and spikes, the noise floor was significantly reduced and more accurate estimates of the turbulent velocity variance were obtained.

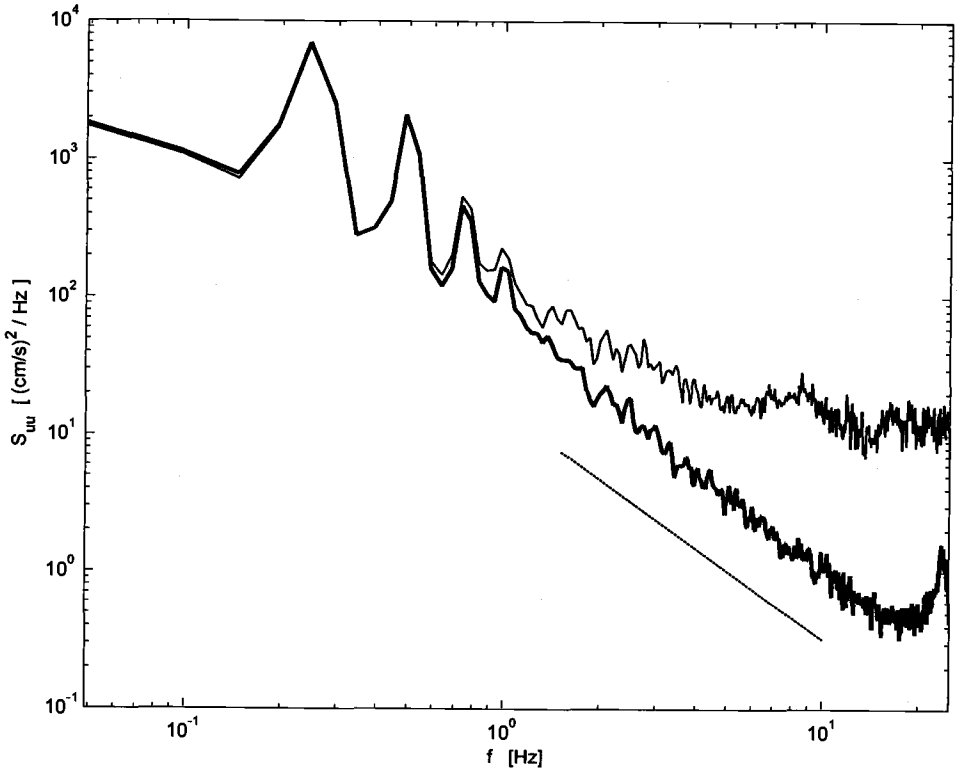

Figure 2.3. Typical raw (light) and despiked (heavy) cross-shore velocity spectra. Data are from the regular wave case P4, 34 cm above the bed. -5/3 slope added for reference (--).

Doppler noise, white noise present at all frequencies, is inherent in all coherent Doppler velocimeters and can significantly bias velocity variance estimates (Nikora and Goring 1998). After removing signal dropouts and spikes, the magnitude of the Doppler noise floor was estimated from the high-frequency portion of the spectrum and integrated over the frequency range used to estimate the variance. This yielded an estimate of the noise contribution to the variance, and was subtracted from the total variance prior to estimating turbulent quantities, such as $\overline{k}$.

Finally, velocity data were filtered to remove noise from high-frequency instrument vibration caused by breaking waves hitting the 40 cm stem on the ADVs and the supports used to deploy the ADVs in the flume. Noise due to vibration of the ADV stem was present in the u and v components of velocity and centered at 24 Hz, as shown in the despiked spectrum in Figure 2.3. In the u component of velocity, a 7th order Chebyshev type II low-pass filter with a corner frequency of 20 Hz was used to remove this noise from the record. Vibration from the supports used to deploy the ADVs was only present in the v component of velocity and occurred at frequencies between 12 – 20 Hz. A 6th order filter of the same type with a cutoff frequency of 10 Hz was used to remove this noise along with the noise from the ADV stem vibration from v. The w component of velocity was unaffected by any vibration and was not filtered.

Accounting for these sources of noise significantly reduced estimates of $\bar{k}$ for both the random and regular wave cases. The average percent reduction in $\bar{k}$ for all of the measurements was 27%, 52%, and 22% for the ensemble averaging, high-pass filtering, and differencing methods, respectively. [A more detailed explanation of the post-processing of velocity time series can be found in Appendix B.2.]

2.6 Application of the Turbulence Separation Methods

Each of the three methods described in Section 2.3 were applied to the post-processed data using the following procedures. The ensemble averaging technique was applied to

the regular wave case by separating individual waves using a zero-upcrossing technique, scaling the wave period to $T = 4.0$ s, then computing the wave component of velocity. This was to ensure that the velocity was averaged relative to the same point in the wave phase because the wave period in the surf zone varies slightly, even when running regular waves (Svendsen 1987). Additionally, low-frequency fluctuations in the velocity that would have been recorded as turbulent velocities ("pseudo-turbulence") were removed by high-pass filtering the raw signal at 0.0625 Hz (one-quarter of the peak wave frequency) prior to ensemble averaging. After calculating the wave component of velocity, the turbulent component was estimated by subtracting the wave component from the total velocity between the zero-crossings used to separate each wave. The ensemble averaging technique was also applied to one elevation of the random wave case by repeating the same random time series 7 times at P5 with all three ADVs 32 cm above bed (21 realizations). In this case, each time series was treated as a "wave" and the procedure described above was applied.

The high-pass filter selected to isolate turbulent motions from wave-induced motions was a 7th order Chebyshev type II filter with a cutoff frequency of 1 Hz. This cutoff was chosen based on visual inspection of the low-frequency end of the -5/3 slope in the power spectral density of the observed cross-shore velocity. A cutoff of 1 Hz also corresponds to 4 times the peak wave frequency, and is lower than the cutoff of Nadaoka *et al.* (1989) who used approximately 7 times the peak wave frequency.

The results obtained using this method are highly sensitive to the cutoff chosen and it was found that increasing it by a factor of 2 reduced the magnitude of $\bar{k}$ by 40% in both the random and regular wave cases.

As described earlier, the method of Trowbridge (1998) requires that the waves be unidirectional. This assumption was valid offshore (P1-P3) and for the breaking region over the bar crest (P4-P6) in the random and regular wave cases. However, during regular wave runs, the waves were not alongshore uniform in the inner surf zone (P7). This alongshore partial standing wave was not observed for waves with longer periods ($T = 7$ s) that would break continuously from the bar crest to the shoreline, or for waves with shorter periods ($T = 2$ s) that would quickly reform after breaking on the bar. Due to these alongshore inhomogeneities in the inner surf zone, differencing estimates should be treated with caution at P7, and it is noted that all three methods estimated little turbulent kinetic energy at this location.

[Examples of the application of all three methods in the time and frequency domains are included in Appendix C along with illustrations of the potential sources of error.]

2.7 Comparison of Turbulence Separation Methods

To illustrate the application of each method to a typical time series, Figure 2.4 shows the temporal variation of u and k, where k is the time-dependent turbulent kinetic energy per unit mass. Data are from the regular wave case at P5, 10.4 cm above the

bed. In this figure, the ensemble averaging and high-pass filtering methods were applied to ADV A500 and the differencing method was applied to A500 and A507. It is noted that the ensemble averaging and high-pass filtering methods estimated k at a single location, whereas the differencing method estimated the average value of k between the two sensors. The time-averaged value of k for the entire time series, equal to $\bar{k}$ for the ADVs used, is also shown with a horizontal dashed line.

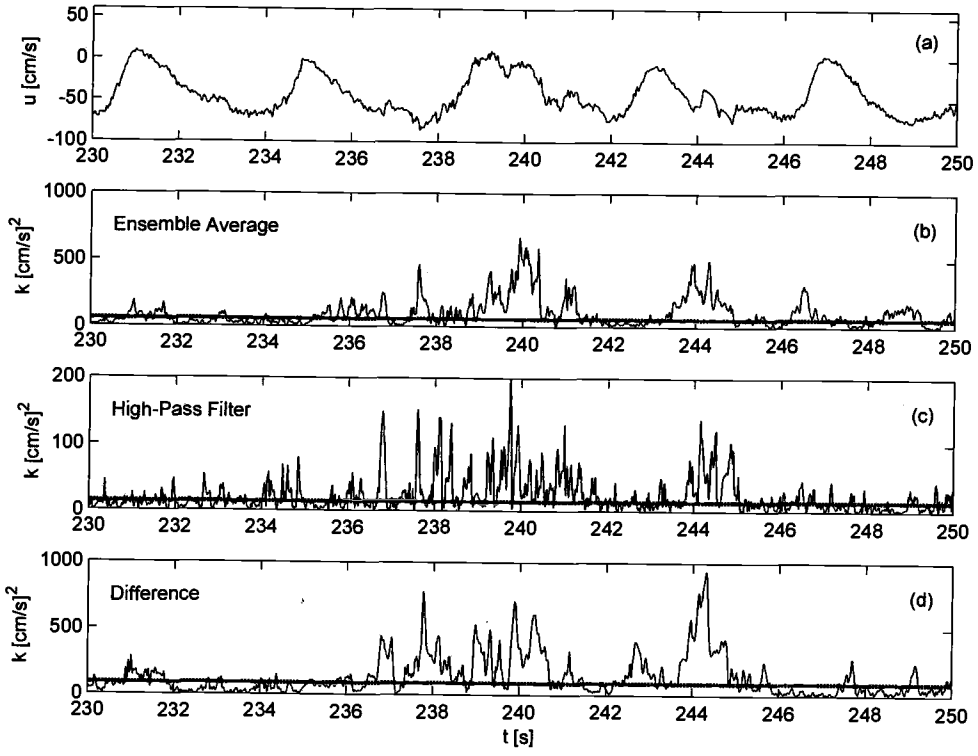

Figure 2.4. Time variation of u (a) and k from the ensemble averaging (b), high-pass filtering (c), and differencing methods (d). Average k for the time series indicated by (--). Data are from the regular wave case, P5, 10.4 cm above the bed, using ADV A500 for (a-c) and A500 and A507 for (d).

In this figure we see that the magnitude of k was similar where the ensemble averaging and differencing methods were applied, and both were about five times larger than the values from high-pass filtering (note the change in y-axis scale). Furthermore, despite the regular forcing, all three methods exhibited an intermittent nature, whereby the instantaneous value of k was an order of magnitude larger than the average value, as observed by Cox and Kobayashi (2000). The signatures from the ensemble averaging and differencing methods were qualitatively similar and made up of a few large events, whereas the signature from high-pass filtering contained many more short events. This difference is attributed to the fact that the high-pass filtered data only contained energy at frequencies greater than 1 Hz. A detailed study of the intermittent properties is left for future work.

To provide a synoptic picture of how the separation method affected the magnitude and spatial structure of the turbulence, estimates of $\bar{k}$ from each method were compared. For the random wave case, $\bar{k}$ was estimated independently using each ADV, and the value reported herein is the average of the three. The same procedure was followed for the regular wave case, but only ADVs A500 and A507 were used because of problems with the synchronization of A595. It is important to note that it is impossible to compare the results of each method to the true value; therefore, we can only indicate whether each method consistently provides a low/high estimate and assume that the true value lies somewhere among the three. [The alongshore variation of $\bar{k}$ was not significant and the details are included in Appendix D.]

Figure 2.5 shows the vertical variation of $\overline{k}$ estimated using all three methods at P4 – P6 for the random and regular wave cases. In both cases the high-pass filter provided a low estimate of $\overline{k}$, despite the fact that a lower cutoff than Nadaoka *et al.* (1989) was used. This was most likely due to energy neglected from large eddies with frequencies lower than 1 Hz, and is consistent with the comparisons made by Svendsen (1987).

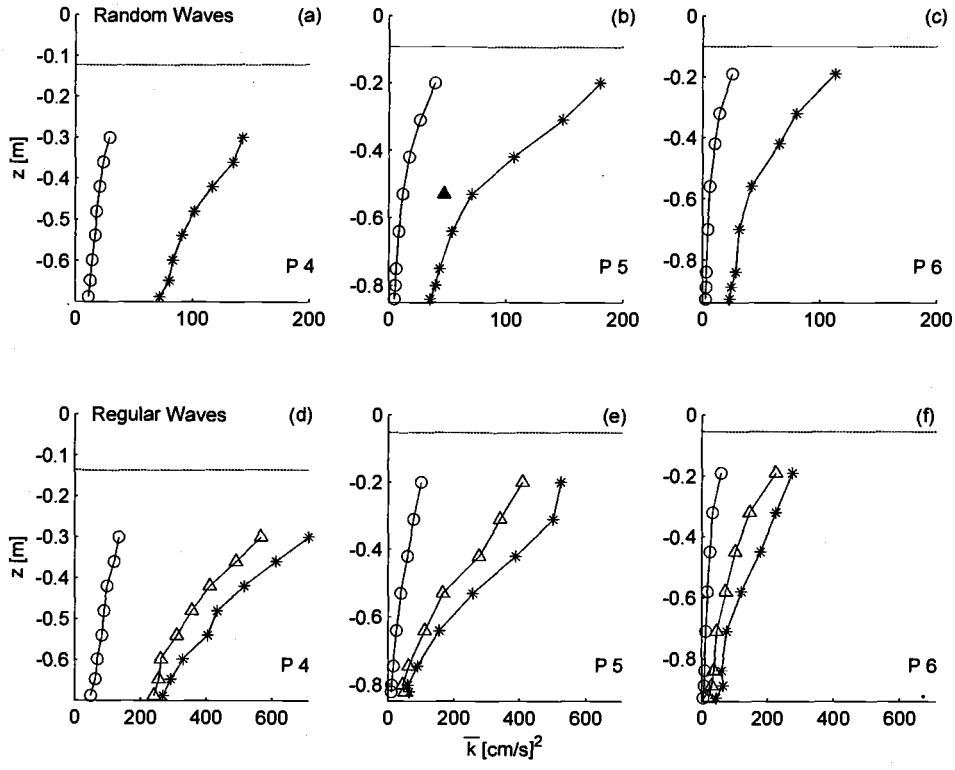

Figure 2.5. Vertical variation of $\overline{k}$ for random (a-c) and regular (d-f) waves at P4 - P6 using ensemble averaging (Δ), high-pass filtering (o), and differencing (*) techniques. Ensemble averaging estimate from the repeated random wave runs included at P5 (▲). Trough level indicated by (--), bottom of the figure indicates the fixed bed.

In the regular wave case, $\bar{k}$ estimates from the differencing method were approximately 26% larger than the ensemble averaging values. If ensemble averaging is considered to be a well-defined way to separate wave-induced and turbulent motions for regular waves, then these results indicate that the differencing method can be used to reasonably estimate $\bar{k}$ in the presence of regular waves. This can be extended to random waves as well, because this method does not require that the waves are repeatable. This conclusion is supported by the ensemble averaging estimate for the repeated random runs at P5.

The vertical variation of $\bar{k}$, shown in Figure 2.5, was similar among all three methods, indicating that the structure of $\bar{k}$ was not affected by the method used to extract the turbulent signal. This is verified in Figure 2.6, where scatter plots of $\bar{k}$ estimated using each method show that the three methods are linearly correlated in both the random and regular wave cases ($r^2 > 0.93$). Data from P3 were not included here because the high-pass filtering estimates were significantly biased by wave harmonics above 1 Hz at P3 due to the highly nonlinear waves near the onset of breaking.

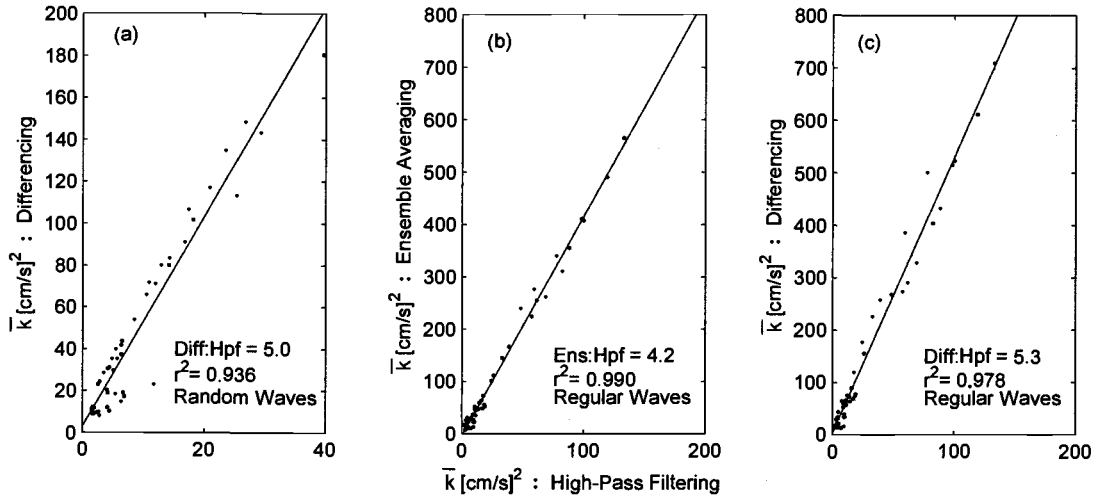

Figure 2.6. Scatter plot of $\bar{k}$ obtained from: differencing and high-pass filtering for random waves (a), ensemble averaging and high-pass filtering for regular waves (b), and differencing and high-pass filtering for regular waves (c). Slope of the best fit line and r^2 value shown on plot.

2.8 Turbulence Observations Over the Bar

2.8.1 Cross-Shore and Vertical Variation of $\bar{k}$

Figure 2.7 shows the cross-shore and vertical variation of $\bar{k}$, where the estimates from ensemble averaging and differencing have been scaled to the high-pass filtering estimate using the ratios (slopes) given in Figure 2.6 (i.e. for the random wave case, all differencing estimates were divided by 5.0). All three methods show the same vertical and cross-shore variation, which gives us confidence that the observed structure of $\bar{k}$ is accurate.

In the region where waves were breaking (P4-P6), estimates of $\bar{k}$ were largest near trough level and decayed with depth, as expected. Directly over the bar crest (P4), $\bar{k}$ was significant throughout the water column, even 1 cm above the bed. Interestingly, this seems to be a localized feature, as only a few meters onshore (P5), $\bar{k}$ was confined to the upper portion of the water column, a trend that continued onshore. Approximately 1.5 wavelengths onshore of the bar crest (P7) there was very little turbulence within the water column, consistent with observations that the waves had reformed at this location. Offshore of the bar crest (P3), estimates from the ensemble averaging and differencing techniques suggest that turbulence generated at P4 may have been advected offshore and confined to a region near the bottom. This is the only location where the maximum value of $\bar{k}$ was not near trough level. Offshore of breaking (P2) $\bar{k}$ was approximately zero and provides an indication of the noise level in our estimate of $\bar{k}$. Estimates from P1 were also near zero and not included in Figure 2.7. [Estimates from P1 are included in Appendix D for completeness.]

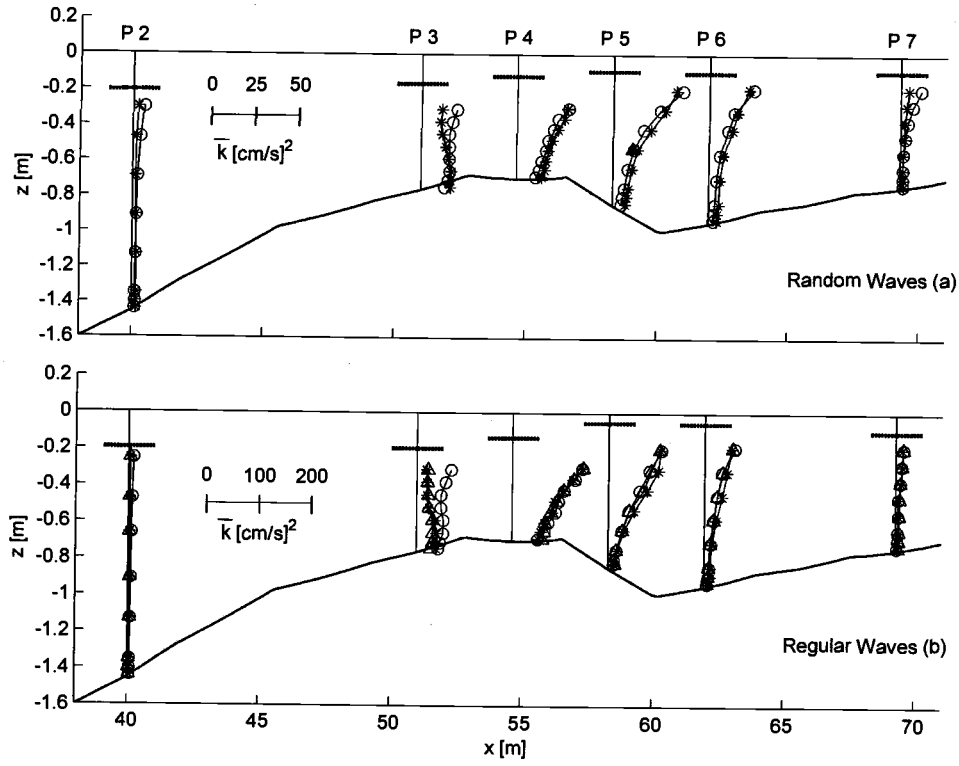

Figure 2.7. Cross-shore and vertical variation of $\bar{k}$ for the random (a) and regular (b) wave cases using ensemble averaging estimates divided by 4.2 (Δ), high-pass filtering estimates (o), and differencing estimates divided by 5.0 (random) and 5.3 (regular) (*). Ensemble averaging estimate from the repeated random wave runs divided by 4.2 included at P5 (▲). Trough level indicated by (--).

It is interesting to note that in the regular wave case, $\bar{k}$ estimated 1 cm above the bed was an order of magnitude larger at P4, where wave breaking was intense, than at P2 and P7, where the waves were not breaking. If the increase in $\bar{k}$ at P4 was due to boundary layer processes, we would expect it to be accompanied by a large change in the peak near bottom wave velocity. However, the peak wave velocity measured 1 cm above the bed at P4 was only 25% less than the velocity at P2 and 2% less than

the velocity at P7, far from an order of magnitude change. This, along with the vertical variation of $\bar{k}$, suggests that the increase in near-bed turbulent kinetic energy at P4 was due to turbulence generated by breaking waves at the surface that was transported to the bed, and not bottom boundary layer processes.

Although the structure of the turbulence was similar for the random and regular wave cases, the magnitude of $\bar{k}$ was significantly smaller in the random wave case (approximately 5 times smaller at P4), despite similar offshore wave conditions. This is most likely due to inherent differences in the wave breaking properties for regular and random wave fields. For example, the reviewers noted that the surf zone created in the random wave case was broader than in the regular wave case. This allowed the wave energy to be dissipated within a larger volume of water and reduced the average turbulent energy observed at a fixed point in the water column. Additionally, the percentage of waves that broke over the bar was smaller in the random wave case because it contained waves that were small enough to propagate over the bar without breaking. A portion of the difference observed by George *et al.* (1994) between scaled estimates of turbulence intensity obtained from laboratory tests using regular waves and field observations where random seas exist may be explained by the difference observed here in the random and regular wave cases along with the fact that different methods were used to separate the wave-induced and turbulent components of velocity in the lab and field tests.

2.8.2 Local Isotropy

The isotropy of the turbulence was analyzed in the region where large turbulent velocities were observed (P4, P5, P6 – only elevations greater than 10 cm above the bed). Table 2.2 shows the ratio of the three components of the velocity variance to $2\bar{k}$ for the random and regular wave cases using all three separation methods. This indicates the relative importance of each component of the variance to $\bar{k}$. Values from other characteristic flows are provided as a reference (Svendsen 1987).

Table 2.2. Isotropy of the average turbulence in the upper water column where wave breaking was observed. Values are the ratio of the average turbulent velocity variance to $2\bar{k}$, where the averaging is applied to all measurements greater than 10 cm above the bed. Data for other flows are from Svendsen (1987).

		P4			P5			P6		
	Method	$\overline{u'u'}$	$\overline{v'v'}$	$\overline{w'w'}$	$\overline{u'u'}$	$\overline{v'v'}$	$\overline{w'w'}$	$\overline{u'u'}$	$\overline{v'v'}$	$\overline{w'w'}$
Random	High-Pass Filter	0.40	0.30	0.30	0.36	0.32	0.32	0.35	0.31	0.34
	Ensemble Average	-	-	-	0.38	0.34	0.28	-	-	-
	Differencing	0.48	0.31	0.21	0.45	0.32	0.23	0.46	0.29	0.25
Regular	High-Pass Filter	0.34	0.34	0.32	0.33	0.35	0.32	0.34	0.33	0.33
	Ensemble Average	0.42	0.33	0.25	0.40	0.34	0.26	0.38	0.34	0.29
	Differencing	0.47	0.32	0.21	0.49	0.30	0.21	0.48	0.29	0.23
Other Flows	Homogen. Isotrop.	0.33	0.33	0.33						
	Plane Wake	0.42	0.26	0.32						
	Bound. Layer (inner)	0.62	0.28	0.10						

From this table we see that the ensemble averaging and differencing methods consistently produced turbulence estimates that were not isotropic and were dominated

by the cross-shore component of the variance $\left(\overline{u'u'}\right)$. This is similar to a plane wake, but unlike a plane wake, the vertical component $\left(\overline{w'w'}\right)$ was the least important. Estimates from the high-pass filtering method were not consistent with the other two methods, despite the similarities observed in the structure of $\bar{k}$. This suggests relatively large anisotropy in the lower-frequency (less than 1 Hz) observed fluid motions compared to higher-frequency (greater than 1 Hz) fluid motions. The similarities observed between the ensemble averaging and differencing methods further indicates that these methods can be used to analyze the details of wave breaking turbulence. In every case, the near-bed turbulence (less than 10 cm above the bed) was anisotropic due to confinement of the vertical component of the variance by proximity to the bed.

2.9 Conclusions

Data obtained as part of a large-scale laboratory experiment to study the turbulence generated by waves breaking on a fixed barred beach were presented. This data set included synoptic measurements of the fluid velocity and free surface elevation for one random and one regular wave case. The fluid velocity was measured at 7 locations within the cross-shore. At each location 8 points were measured in the vertical direction, beginning 1 cm above the bed and extending to approximately trough level.

An analysis of the cross-shore and vertical variation of the time-averaged turbulent kinetic energy per unit mass $(\bar{k})$ showed that:

1. Wave breaking turbulence was largest at the bar crest (P4) and influenced the entire water column, indicating that it may be important for near-bed processes on a barred beach, even in a time-averaged sense. Landward of the bar (P5, P6) the turbulence was confined to the upper layer and had dissipated once the waves reformed (approximately 1.5 wavelengths onshore of the bar crest, P7).
2. The cross-shore and vertical structure of the turbulence was similar in the random and regular wave cases. However, the magnitude of $\bar{k}$ in the regular wave case was as much as 5 times larger than the random case, despite similar offshore wave conditions.
3. The magnitude of $\bar{k}$ varied by as much as a factor of 5 based on the method used to separate the wave-induced and turbulent velocities, but the cross-shore and vertical structure of $\bar{k}$ was independent of the method used.
4. The differencing method proposed by Trowbridge (1998) appeared to be the most promising as it agreed closely with ensemble averaging and can be applied to random wave fields. This agreement was both in terms of the magnitude and structure of time-averaged quantities ($\bar{k}$ and isotropy), and in the signature of the time-dependent turbulent kinetic energy.

These observations are an important step toward understanding the dynamics of nearshore turbulence. Future work will be aimed at addressing not only the

mechanisms responsible for the vertical and cross-shore transport of the turbulence generated by wave breaking, but also the contribution of shear production to the total turbulent energy within the surf zone and the rate of turbulent dissipation (e.g., Ting and Kirby 1995). We plan to investigate the intermittency observed in k and the effect that intense wave breaking events have on velocities averaged over several wave periods. [The preliminary results of this analysis are included in Appendix E.] Our observations may also be used to aid in the development of numerical models aimed at predicting the detailed hydrodynamics of waves breaking over a barred beach.

2.10 Acknowledgments

This work was partially funded by the National Science Foundation under grants No. CMS-0086571, EEC-0244205, and OCE-0351741. The authors would like to thank Terry Dibble and Emi Fujii for their work in setting up and conducting the experiment as well as the valuable discussions with Dr. Merrick Haller and Dr. Tuba Özkan-Haller.

2.11 References

Battjes, J.A. 1974. Surf Similarity, *Proc. 14th Int. Conf. on Coastal Eng.*, ASCE, 466-480.

Bowen, A.J., D.L. Inman, and V.P. Simmons. 1968. Wave 'set-down' and 'set-up,' *J. Geophys. Res.*, 73 (8), 2569-2577.

Cox, D.T. and N. Kobayashi. 2000. Identification of intense, intermittent coherent motions under shoaling and breaking waves, *J. Geophys. Res.*, 105 (C6), 14223-14236.

Cox, D.T., N. Kobayashi, and A. Okayasu. 1995. Experimental and numerical modeling of surf zone hydrodynamics, *Res. Report CACR-95-07 (Ph.D. dissertation of 1st author)*, Center for Applied Coastal Research, Univ. of Delaware, pp. 293.

Elgar, S., B. Raubenheimer, and R.T. Guza. 2001. Current Meter Performance in the Surf Zone, *J. Atmos. Oceanic Technol.*, 18, 1735-1746.

Fredsøe, J., and R. Deigaard. 1992. *Mechanics of Coastal Sediment Transport,* World Scientific Publishing, Singapore, pp. 369.

Garcez Faria, A.F.G., E.B. Thornton, T.C. Lippmann, and T.P. Stanton. 2000. Undertow over a barred beach, *J. Geophys. Res.*, 105 (C7), 16999-17010.

George, R., R.E. Flick, and R.T. Guza 1994. Observations of turbulence in the surf zone, *J. Geophys. Res.*, 99 (C1), 801-810.

Goda, Y. 2000. *Random Seas and Design of Maritime Structures (2nd Edition)*, World Scientific Publishing, London, pp. 443.

Goring, D.G., and V.I. Nikora. 2002. Despiking acoustic Doppler velocimeter data, *J. Hydraul. Eng.*, 128 (1), 117-126.

Hattori, M., and T. Aono. 1985. Experimental study on turbulence structures under spilling breakers, in *The Ocean Surface*, edited by Y. Toba and H. Mitsuyasu, 419-424.

Hoefel, F., and S. Elgar. 2003. Wave-induced sediment transport and sandbar migration, *Science*, 299, 1885-1887.

Jonsson, I.G. 1966. Wave boundary layers and friction factors, *Proc. 10th Int. Conf. on Coastal Eng.*, ASCE, 127-148.

Nadaoka, K., M. Hino, and Y. Koyano. 1989. Structure of the turbulent flow field under breaking waves in the surf zone, *J. Fluid Mech.*, 204, 359-387.

Nadaoka, K., and T. Kondoh. 1982. Laboratory measurements of velocity field structure in the surf zone by LDV, *Coastal Eng. in Japan*, 25, 125-146.

Nikora, V.I., and D.G. Goring. 1998. ADV measurements of turbulence: Can we improve their interpretation?, *J. Hydraul. Eng.*, 124 (6), 630-634.

Sancho, F., P.A. Mendes, J.A. Carmo, M.G. Neves, G.R. Tomasicchio, R. Archetti, L. Damiani, M. Mossa, A. Rinaldi, X. Gironella, and A.S. Arcilla. 2001. Wave hydrodynamics over a barred beach, *Proc. Waves 2001*, ASCE, 1170-1179.

Stive, M.J.F. 1980. Velocity and pressure field in spilling breakers, *Proc. 17th Int. Conf. on Coastal Eng.*, ASCE, 1, 547-566.

Stive, M.J.F., and H.G. Wind. 1982. A study of radiation stress and set-up in the nearshore region, *Coastal Eng.*, 6, 1-25.

Svendsen, I.A. 1987. Analysis of surf zone turbulence, *J. Geophys. Res.*, 92 (C5), 5115-5124.

Thornton, E.B., R.A. Dalrymple, T. Drake, E. Gallagher, R.T. Guza, A. Hay, R.A. Holman, J. Kaihatu, T.C. Lippmann, and T. Özkan-Haller. 2000. State of nearshore processes research: II, *Technical Report NPS-OC-00-001*, Naval Postgraduate School, Monterey, CA, 37 pp.

Ting, F.C.K., and J.T. Kirby. 1994. Observation of undertow and turbulence in a laboratory surf zone, *Coastal Eng.*, 24, 51-80.

Ting, F.C.K., and J.T. Kirby. 1995. Dynamics of surf-zone turbulence in a strong plunging breaker, *Coastal Eng.*, 24, 177-204.

Trowbridge, J. 1998. On a technique for measurement of turbulent shear stress in the presence of surface waves, *J. Atmos. Oceanic Technol.*, 15, 290-298.

Trowbridge, J., and S. Elgar. 2001. Turbulence measurements in the surf zone, *J. Phys. Oceanogr.*, 31, 2403-2417.

3. General Conclusions

This thesis presented the details of a large-scale laboratory experiment designed to study the turbulence generated by waves breaking on a fixed barred beach. Prototype-scale laboratory experiments can improve our understanding of the turbulence generated by breaking waves and the potential influence that it has on sediment transport in the nearshore. The data set included synoptic measurements of the fluid velocity and free surface elevation for one random and one regular wave case. In each case, the fluid velocity was measured at 7 locations within the cross-shore. At each location, 8 points were measured in the vertical direction, beginning 1 cm above the bed and extending to approximately trough level.

An analysis of the cross-shore and vertical variation of the time-averaged turbulent kinetic energy per unit mass $(\bar{k})$ showed that in the region where waves were breaking (P4-P6), estimates of $\bar{k}$ were largest near trough level and decayed with depth, consistent with small-scale laboratory observations (e.g., Svendsen 1987). Directly over the bar crest (P4), wave breaking turbulence influenced the entire water column, resulting in large estimates of $\bar{k}$ 1 cm above the bed. This indicates that even in a time-averaged sense, wave breaking turbulence may be important for near-bed processes on a barred beach. Landward of the bar (P5, P6) the turbulence was confined to the upper layer and dissipated once the waves had reformed (approximately 1.5 wavelengths onshore of the bar crest, P7). This structure was

similar in the random and regular wave cases; however, estimates of $\bar{k}$ were as much as 5 times larger in the regular wave case, despite similar offshore wave conditions. This may partially explain the difference in magnitude observed by George *et al.* (1994) between scaled estimates of turbulence intensity obtained from small-scale laboratory tests using regular waves and field tests where random seas exist.

Three methods were used to separate the wave-induced and turbulent components of velocity: ensemble averaging, high-pass filtering, and a differencing method proposed by Trowbridge (1998). Qualitatively, the cross-shore and vertical structure of $\bar{k}$ was independent of the method used; however, the magnitude of $\bar{k}$ varied by as much as a factor of 5 between the methods. The differencing method agreed closely with ensemble averaging in terms of the magnitude and structure of time-averaged quantities, and in the signature of the time-dependent turbulent kinetic energy. Given this agreement and the general acceptance of ensemble averaging as an appropriate method to separate wave-induced and turbulent components of velocity for regular waves (Svendsen 1987), the differencing method appears to be the most suitable for application to random waves, such as those observed in the field.

These observations are an important step toward understanding the dynamics of nearshore turbulence. Future work will be aimed at addressing not only the mechanisms responsible for the vertical and cross-shore transport of the turbulence

generated by wave breaking, but also the contribution of shear production to the total turbulent energy within the surf zone and the rate of turbulent dissipation (e.g., Ting and Kirby 1995). We plan to investigate the intermittency observed in k and the effect that intense wave breaking events have on velocities averaged over several wave periods. Our observations may also be used to aid in the development of numerical models aimed at predicting the detailed hydrodynamics of waves breaking over a barred beach. Additionally, we plan to use our observations to drive the two-phase sediment transport model of Hsu *et al.* (2004) including a source of turbulent kinetic energy from wave breaking at the upper boundary to investigate the effect that wave breaking turbulence has on the suspension and entrainment of sediment.

Bibliography

Battjes, J.A. 1974. Surf similarity, *Proc. 14th Int. Conf. on Coastal Eng.*, ASCE, 466-480.

Bowen, A.J., D.L. Inman, and V.P. Simmons. 1968. Wave 'set-down' and 'set-up,' *J. Geophys. Res.*, 73 (8), 2569-2577.

Cox, D.T., and N. Kobayashi. 2000. Identification of intense, intermittent coherent motions under shoaling and breaking waves, *J. Geophys. Res.*, 105 (C6), 14223-14236.

Cox, D.T., N. Kobayashi, and A. Okayasu. 1994. Vertical variations of fluid velocities and shear stress in surf zones, *Proc. 24th Int. Conf. on Coastal Eng.*, ASCE, 1, 98-112.

Cox, D.T., N. Kobayashi, and A. Okayasu. 1995. Experimental and numerical modeling of surf zone hydrodynamics, *Res. Report CACR-95-07 (Ph.D. dissertation of 1st author)*, Center for Applied Coastal Research, Univ. of Delaware, 293 pp.

Cox, D.T., N. Kobayashi, and A. Okayasu. 1996. Bottom shear stress in the surf zone, *J. Geophys. Res.*, 101 (C6), 14337-14348.

Dette, H.H., M. Larson, J. Murphy, J. Newe, K. Peters, A. Reniers, and H. Steetzel. 2002. Application of prototype flume tests for beach nourishment assessment, *Coastal Eng.*, 47, 137-177.

Elgar, S., B. Raubenheimer, and R.T. Guza. 2001. Current meter performance in the surf zone, *J. Atmos. Oceanic Technol.*, 18, 1735-1746.

Fredsøe, J., and R. Deigaard. 1992. *Mechanics of Coastal Sediment Transport,* World Scientific Publishing, Singapore, 369 pp.

Garcez Faria, A.F.G., E.B. Thornton, T.C. Lippmann, and T.P. Stanton. 2000. Undertow over a barred beach, *J. Geophys. Res.*, 105 (C7), 16999-17010.

George, R., R.E. Flick, and R.T. Guza. 1994. Observations of turbulence in the surf zone, *J. Geophys. Res.*, 99 (C1), 801-810.

Goda, Y. 2000. *Random Seas and Design of Maritime Structures (2nd Edition)*, World Scientific Publishing, London, 443 pp.

Goring, D.G., and V.I. Nikora. 2002. Despiking acoustic Doppler velocimeter data, *J. Hydraul. Eng.*, 128 (1), 117-126.

Hattori, M., and T. Aono. 1985. Experimental study on turbulence structures under spilling breakers, in *The Ocean Surface*, edited by Y. Toba and H. Mitsuyasu, 419-424.

Hoefel, F., and S. Elgar. 2003. Wave-induced sediment transport and sandbar migration, *Science*, 299, 1885-1887.

Hsu, T.J., J.T. Jenkins, and P.L.F. Liu. 2004. On two-phase sediment transport: sheet flow of massive particles, *Proc. R. Soc. Lond.*, 460, 2223-2250.

Jonsson, I.G. 1966. Wave boundary layers and friction factors, *Proc. 10th Int. Conf. on Coastal Eng.*, ASCE, 127-148.

Kraus, N.C., J.M. Smith, and C.K. Sollitt. 1992. SUPERTANK laboratory data collection project, *Proc. 23rd Int. Conf. on Coastal Eng.*, ASCE, 3, 2191-2204.

Nadaoka, K., M. Hino, and Y. Koyano. 1989. Structure of the turbulent flow field under breaking waves in the surf zone, *J. Fluid Mech.*, 204, 359-387.

Nadaoka, K., and T. Kondoh. 1982. Laboratory measurements of velocity field structure in the surf zone by LDV, *Coastal Eng. in Japan*, 25, 125-146.

Nikora, V.I., and D.G. Goring. 1998. ADV measurements of turbulence: Can we improve their interpretation?, *J. Hydraul. Eng.*, 124 (6), 630-634.

Peregrine, D.H., and I.A. Svendsen. 1978. Spilling breakers, bores and hydraulic jumps. *Proc. 16th Int. Conf. on Coastal Eng.*, ASCE, 540-551.

Preliminary report of the U.S. Commission on Ocean Policy. 2004. *Governor's Draft*, Washington, D.C. 514 pp.

Sancho, F., P.A. Mendes, J.A. Carmo, M.G. Neves, G.R. Tomasicchio, R. Archetti, L. Damiani, M. Mossa, A. Rinaldi, X. Gironella, and A.S. Arcilla. 2001. Wave hydrodynamics over a barred beach, *Proc. Waves 2001*, ASCE, 1170-1179.

Scott, C.P., D.T. Cox, S. Shin, and N. Clayton. 2004. Estimates of surf zone turbulence in a large-scale laboratory flume, Submitted to *Proc. 29th Int. Conf. on Coastal Eng.*, ASCE.

SonTek/YSI. 2001. Acoustic Doppler velocimeter principles of operation, SonTek/YSI, Inc., San Diego, CA, 14 pp.

Stive, M.J.F. 1980. Velocity and pressure field in spilling breakers, *Proc. 17th Int. Conf. on Coastal Eng.*, ASCE, 1, 547-566.

Stive, M.J.F., and H.G. Wind. 1982. A study of radiation stress and set-up in the nearshore region, *Coastal Eng.*, 6, 1-25.

Svendsen, I.A. 1987. Analysis of surf zone turbulence, *J. Geophys. Res.*, 92 (C5), 5115-5124.

Thornton, E.B., R.A. Dalrymple, T. Drake, E. Gallagher, R.T. Guza, A. Hay, R.A. Holman, J. Kaihatu, T.C. Lippmann, and T. Özkan-Haller. 2000. State of nearshore processes research: II, *Technical Report NPS-OC-00-001*, Naval Postgraduate School, Monterey, CA, 37 pp.

Ting, F.C.K., and J.T. Kirby. 1994. Observation of undertow and turbulence in a laboratory surf zone, *Coastal Eng.*, 24, 51-80.

Ting, F.C.K., and J.T. Kirby. 1995. Dynamics of surf-zone turbulence in a strong plunging breaker, *Coastal Eng.*, 24, 177-204.

Tomasicchio, G.R., and F. Sancho. 2002. On wave induced undertow at a barred beach, *Proc. 28th Int. Conf. on Coastal Eng.*, World Scientific Publishing, 1, 557-569.

Trowbridge, J. 1998. On a technique for measurement of turbulent shear stress in the presence of surface waves, *J. Atmos. Oceanic Technol.*, 15, 290-298.

Trowbridge, J., and S. Elgar. 2001. Turbulence measurements in the surf zone, *J. Phys. Oceanogr.*, 31, 2403-2417.

Zedel, L., A.E. Hay, R. Cabrera, and A. Lohrmann. 1996. Performance of a single-beam pulse-to-pulse coherent Doppler profiler, *IEEE J. Oceanic Eng.*, 21 (3), 290-297.

APPENDICES

Appendix A. Experimental Setup

A.1 Model Beach Construction

The following section provides additional detail regarding the model beach construction, scale of the experiment, and instrumentation discussed in Section 2.4. Figure A.1 is a schematic of the model bathymetry that was used during the planning and construction of the model beach. It should be noted that the dimensions given in this figure are approximate and it is not to scale.

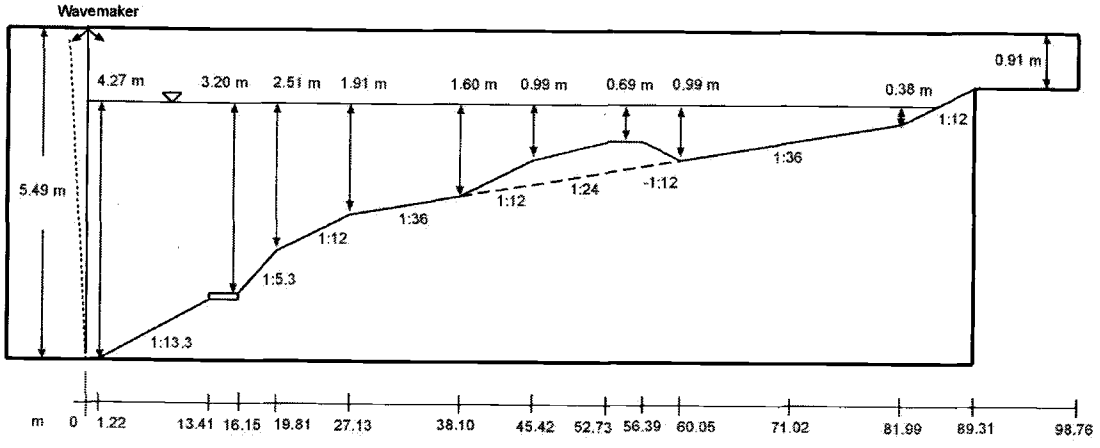

Figure A.1. Schematic of the model bathymetry used during the planning and construction of the model. All dimensions are approximate and the figure is not to scale.

The model bar geometry approximated the bar geometry observed on October 11, 1994, of the DUCK94 field experiment (e.g., Figure 2 Garcez Faria *et al.* 2000) and several key features were compared to estimate the model scale. These are shown in Table A.1 where h_d is defined as the distance from the free surface to the underlying

planar beach at the bar crest, h_{cr} is defined as the depth at the bar crest, h_t is defined as the depth at the bar trough, and w is defined as the width of the bar.

Table A.1. Comparison of the model bar geometry to the average profile observed on October 11, 1994, of the DUCK94 field experiment.

	h_d [m]	h_{cr} [m]	h_t [m]	w [m]
DUCK94	3	2	2.5	100
Model	1.14	0.69	0.99	22
Model:DUCK94	1:3	1:3	1:3	1:5

Table A.1 shows that the model scale was approximately 1:3 and compressed in the cross-shore. This was due to the limitation of the flume length; nevertheless, it captured the hydrodynamic processes of wave breaking and reforming common to natural barred beaches.

The model beach was constructed by fixing concrete slabs (3.7 m x 3.7 m x 0.15 m) to the sidewalls of the flume as shown in Figures A.2 and A.3. The construction was carried out over a three week period by a team of approximately nine students and lab staff. During operation water is present underneath the beach and can flow between each of the concrete slabs. To prevent this, aluminum plates (0.0381 m thick) were fixed over the gaps between each slab and along one of the sidewalls of the flume at every location onshore of $x = 27.13$ m. The slabs were installed flush against the other sidewall of the flume and foam sealant was used to fill small gaps there. Figure A.2 shows these features along with the clips used to secure the beach. It is noted that

these features disturb the flow locally, which is why all of the velocity measurements were carried out more than 1 m from the sidewalls and at the center of each slab (1.8 m from the aluminum seals between the slabs). In the future, I suggest fixing a plate to the bottom of each gap and filling it with foam, because this foam provides a good seal and can be shaped to minimize the flow disturbance.

Figure A.2. Installation of the model beach, looking offshore.

Figure A.3. Completed model beach, looking onshore from approximately P1 (left), and looking offshore from approximately the still water shoreline (right).

Figure A.4 illustrates the breaking type and location for the regular wave case. The fixed wave gage on the left side of the photograph (at the transition in paint) was located at $x = 53$ m. It is clear from these photos that the regular waves were plunging.

Figure A.4. Regular wave beginning to break (right, crest at $x \approx 50$ m) and impinging (left, crest at $x \approx 53$ m).

The instrumentation cart used for collecting velocity profiles is shown in Figures A.5 and A.6 (refer to Figure 2.2 for a schematic). This cart was constructed for this experiment by Terry Dibble, Christopher Scott, and Takayuki Suzuki in one month and cost approximately $5000. All three types of instrumentation used during the experiment are shown in Figure A.5. The three wave gages that moved with the instrument array are shown on the left, the ADV array is shown in the center, and one of the 6 wave gages fixed to the sidewall is shown on the right. Figure A.6 shows the instrumentation cart being used during the experiment.

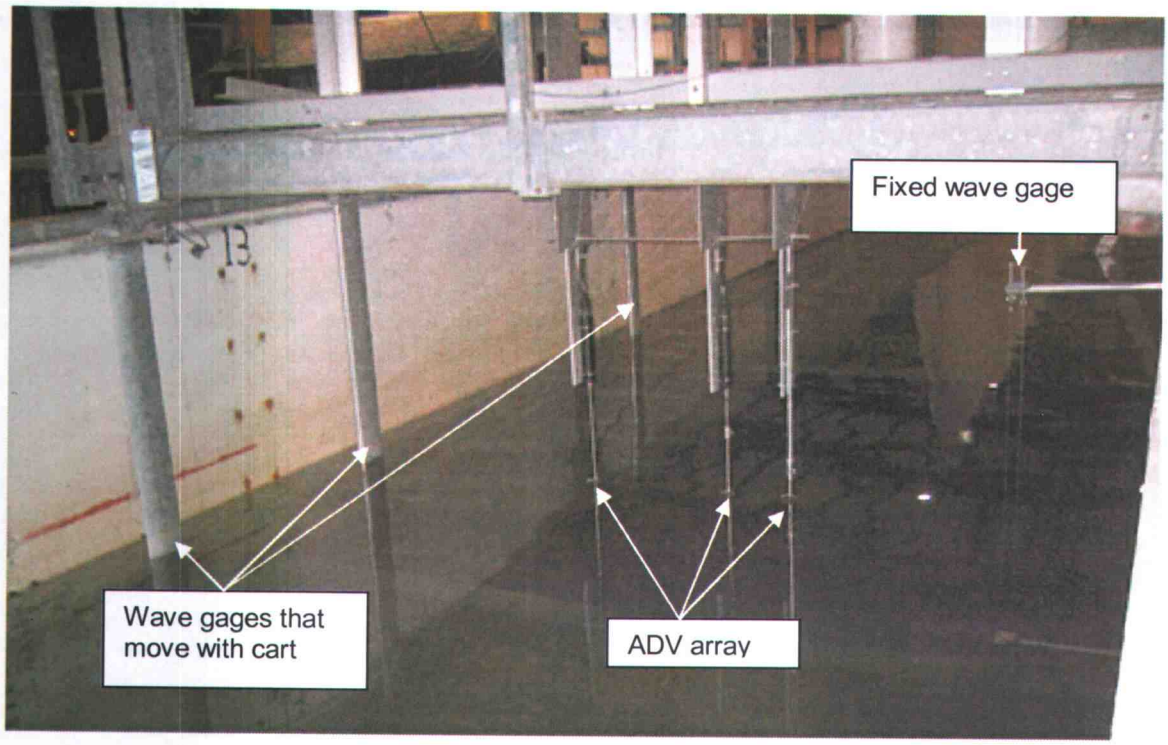

Figure A.5. Movable instrumentation cart (schematic shown in Figure 2.2). The instruments that moved with the cart are shown (3 wave gages, 3 ADVs) along with one fixed wave gage. View is looking onshore.

Figure A.6. Instrumentation cart operating during the experiment.

A.2 Regular Wave Characteristics

Figure A.7 shows the cross-shore variation of H and mean water level ($\overline{\eta}$) for the regular wave case, which was not shown in Section 2.4.2 due to the page limitations of the manuscript. The shoaling ($x < 50$ m), breaking (50 m $< x <$ 60 m), and reforming ($x > 60$ m) regions are clearly shown.

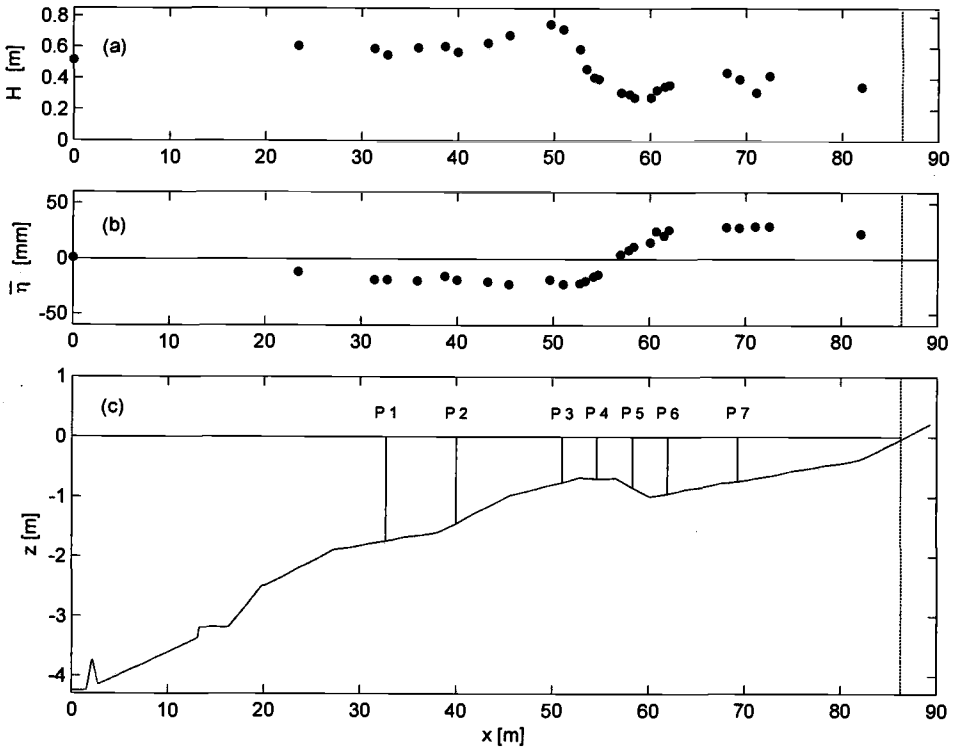

Figure A.7. Cross shore variation of H (a) and $\overline{\eta}$ (b) for the regular wave case. Surveyed bathymetry and locations of velocity profiles P1-P7 (c). Wavemaker located at $x = 0$, still water shoreline indicated by (--).

The variation in H near $x = 70$ m was due to the alongshore partial standing wave discussed in Section 2.6. The variation in H in the shoaling region (30 m $< x <$ 45 m)

was observed during the experiment and thought to be due to a malfunctioning wave gage on the instrumentation cart. Regular wave tests were conducted using a range of wave heights (0.2 m < H < 1.0 m) and periods (2.7 s < T < 8 s) to investigate this possibility. One of the three wave gages on the cart was collocated in the cross-shore with the fixed wave gage at x = 23.45 m, and the suite of wave conditions were run. This process was repeated three times to compare each of the three wave gages on the cart to the fixed wave gage. In every case, the wave height measured using the wave gage on the cart agreed closely with the fixed wave gage (within 2.5 cm or 5% of full scale), indicating that the variation in H observed in the shoaling region was not due to instrument error.

Appendix B. Data Reduction

B.1 Repeatability of the Wave Conditions

Figures B.1 and B.2 illustrate the repeatability of the wave conditions measured seaward of breaking and in the inner surf zone for both the random and regular wave cases. In each figure, the ensemble averaged wave (solid) is shown ± one standard deviation (dash). In the random wave case (Figure B.1), only a portion of the time series is shown, and is representative of the entire 20 minutes.

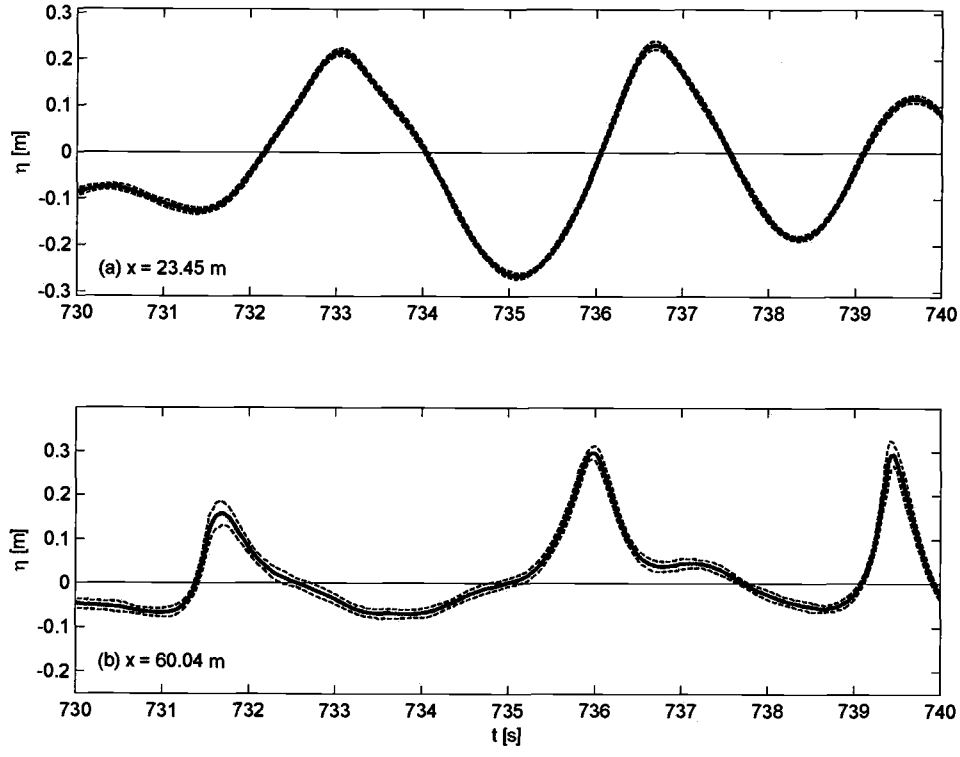

Figure B.1. Ensemble averaged free surface elevation (solid) ± one standard deviation (dash) measured seaward of breaking (a) and in the inner surf zone (b) for the random wave case.

Seaward of breaking the variation in the waveform was very small with an average standard deviation of 0.8 cm and 1.1 cm in the random (Figure B.1a) and regular (Figure B.2a) wave cases, respectively.

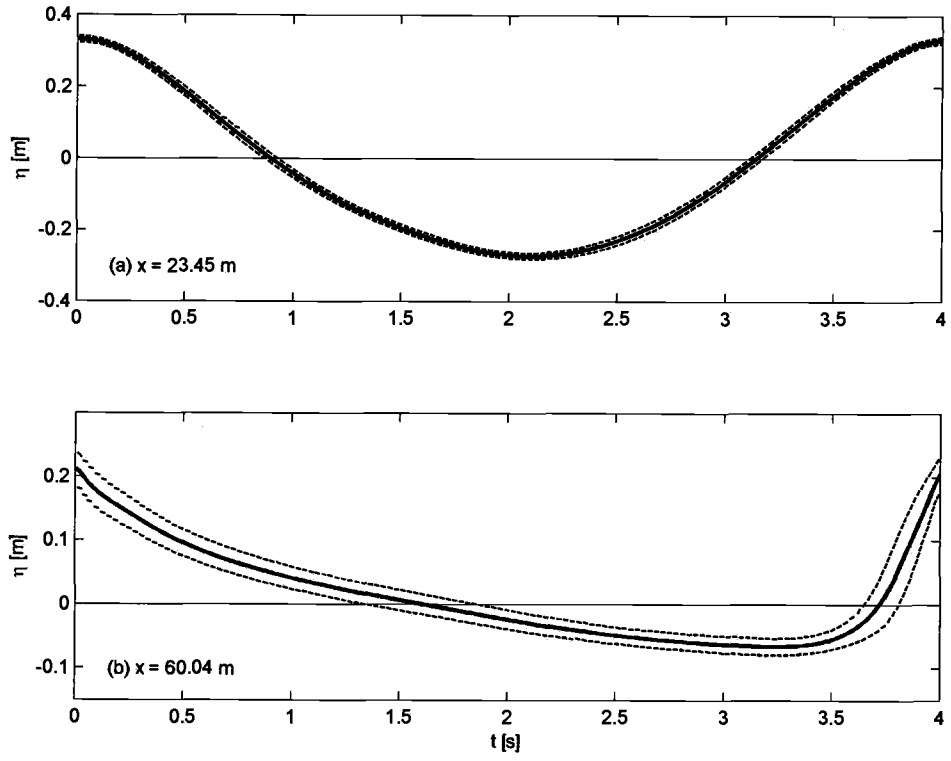

Figure B.2. Ensemble averaged free surface elevation (solid) ± one standard deviation (dash) measured seaward of breaking (a) and in the inner surf zone (b) for the regular wave case.

In the inner surf zone the variation in the waveform was larger due to the presence of wave breaking. The average standard deviation was 1.3 cm and 1.9 cm in the random (Figure B.1b) and regular (Figure B.2b) wave cases, respectively.

B.2 Post-Processing of Velocity Time Series

B.2.1 Signal Dropouts and Spikes

All velocity time series were post-processed to address three sources of noise: signal dropouts and spikes, Doppler noise, and instrument vibration, as discussed in Section 2.5.2. Signal dropouts and spikes were identified using the signal-to-noise ratio (SNR) and correlation values returned by each ADV, along with the phase-space-threshold criterion outlined by Goring and Nikora (2002).

The first two indicators (SNR and correlation) are directly output by the ADV for use in data quality control. The SNR recorded by each ADV is a measure of the intensity of the reflected acoustic signal, and is used to ensure that the reflected signal is stronger than the ambient noise level. SonTek recommends that users maintain a SNR of at least 15 dB for high-resolution measurements and 5 dB for measurements of the mean current (SonTek/YSI 2001). In this test, valid samples were identified as those having an average SNR along all three ADV beams of at least 10 dB. In addition to recording the SNR, each ADV also returns the correlation coefficient, a measure of the correlation between successive acoustic transmissions (pulse-pairs), which provides an instantaneous indicator of the signal quality (Zedel *et al.* 1996). Valid samples were defined as those with an average correlation along all three ADV beams of at least 70%, as recommended by SonTek (SonTek/YSI 2001).

The phase-space-thresholding technique developed by Goring and Nikora (2002) detected abnormally large changes in the magnitude and direction of the velocity that were not identified using the SNR and correlation thresholds. This method utilizes the Universal criterion from normal probability distribution theory, which states that the expected absolute maximum value $(\lambda_U \sigma)$ of a normal, random variable with zero mean and standard deviation σ, is given by:

$$\lambda_U \sigma = \sqrt{2 \ln n}\, \sigma \tag{B.1}$$

where n is the number of samples in the record. Goring and Nikora (2002) observed that when the velocity (u) and its first (Δu) and second derivatives $(\Delta^2 u)$ are plotted in three-dimensional phase-space, good data are clustered in an ellipsoid. Invalid data are identified as those outside of the ellipsoid with bounds given by the expected maximum value along each axis, calculated using Eq. B.1 (e.g., the maximum value along the Δu axis is $\lambda_U \sigma_{\Delta u} = \sqrt{2 \ln n}\, \sigma_{\Delta u}$). The detection of sustained spikes was improved by high-pass filtering the data using a 6th order Chebyshev type II high-pass filter with a cutoff frequency of 1 Hz prior to applying this technique. This was consistent with Goring and Nikora's (2002) suggestion that long-scale fluctuations be removed before applying this method. Figure B.3 illustrates the need for and effectiveness of this technique for a cross-shore velocity time series recorded near the trough level of a non-breaking wave at P1. The samples from t = 170.75 s – 171.25 s are clearly not valid, but were not identified using the SNR and correlation thresholds. These dropouts were most likely due to the phase limitation of the pulse-coherent

processing used by the ADV (SonTek/YSI 2001) and were effectively identified using the phase-space-thresholding method.

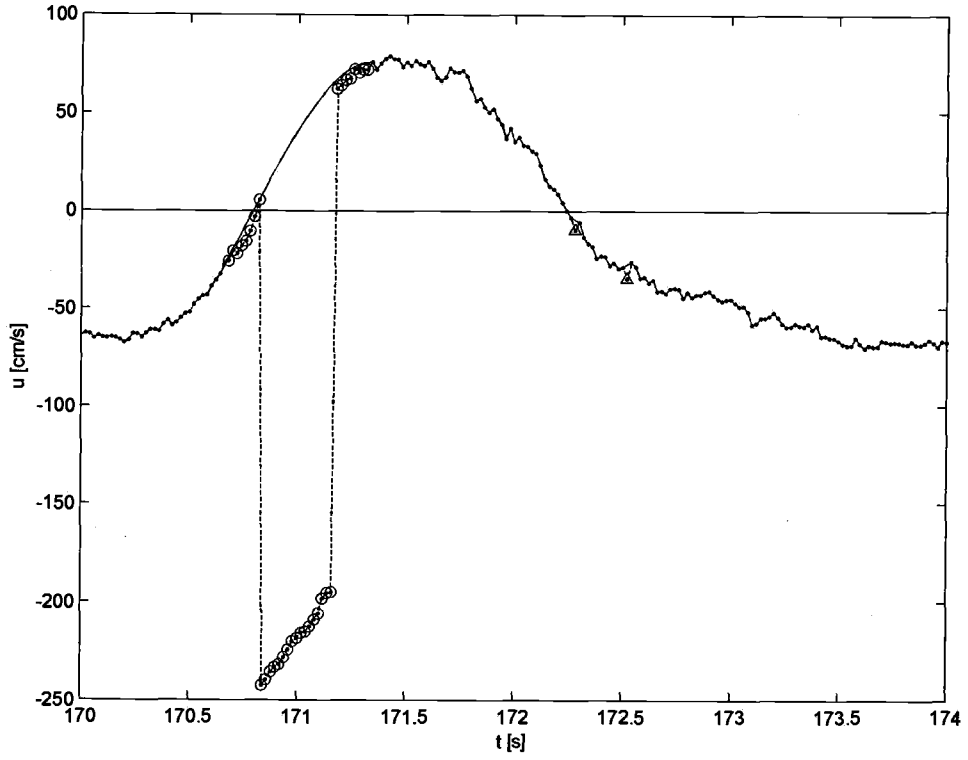

Figure B.3. Example of a sustained signal dropout identified by the phase-space-thresholding method. Raw (dash-dot) and despiked (solid) cross-shore velocity under a non-breaking wave near trough level at P1 are shown from ADV A500. Note that the dropout was identified using phase-space-thresholding (o), not SNR (□) or correlation thresholds (Δ).

Samples identified as invalid by any of the three methods discussed above were replaced using a cubic interpolation tool (Piecewise Cubic Hermite Interpolating Polynomial (pchip), used in MATLAB 7.0®). Visual inspection indicated that this was an appropriate method to replace invalid samples, as shown in Figure B.3, and was very similar to the method suggested by Goring and Nikora (2002) (third-order

polynomial fit to twelve points on either side of the spike). Nobuhito Mori at Osaka City University in Japan provided the MATLAB code and guidance in implementing the phase-space-thresholding technique.

Figures B.4 and B.5 show examples of records with very little and extensive despiking, respectively. In each figure, the total raw (dash) and despiked (solid) time series are shown in the upper panel (a), along with a detailed look at a few waves, including the points identified as invalid by each method, in the lower panel (b).

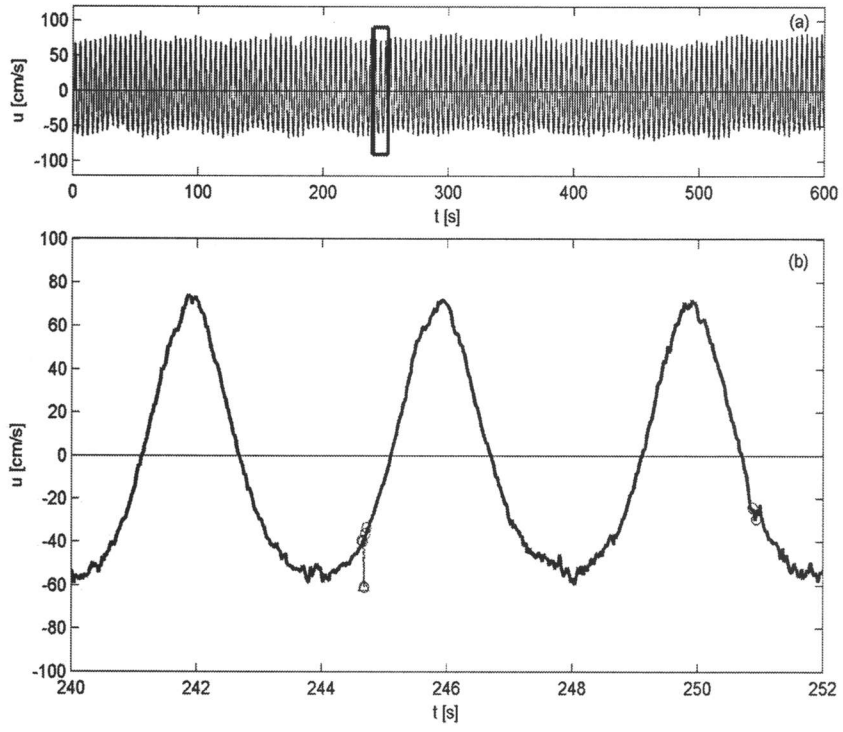

Figure B.4. Example of a velocity time series with very little despiking. Total raw (dash) and despiked (solid) velocity time series are shown (a) along with samples identified as invalid by SNR (□), correlation (Δ), and phase-space (o) thresholds for a few waves (b). Data are from the cross-shore component of velocity from ADV A500, 32 cm above the bed at P2 in the regular wave case.

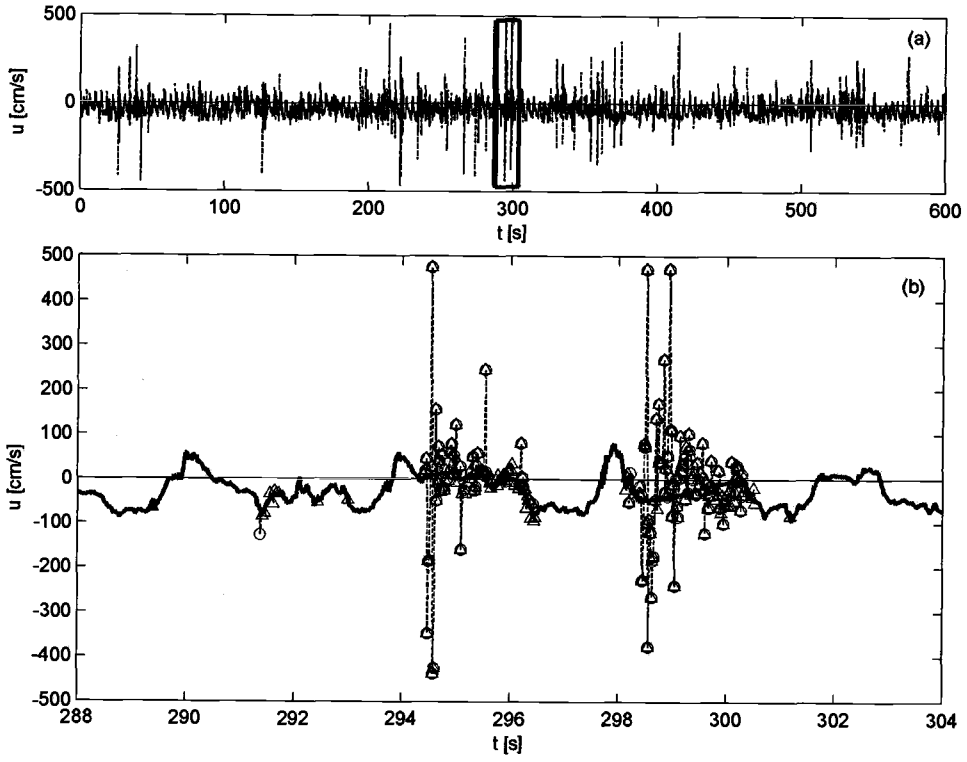

Figure B.5. Example of a velocity time series with extensive despiking. Total raw (dash) and despiked (solid) velocity time series are shown (a) along with samples identified as invalid by SNR (□), correlation (Δ), and phase-space (o) thresholds for a few waves (b). Data are from the cross-shore component of velocity from ADV A507, 1.7 cm above the bed at P3 in the regular wave case.

Tables B.1 - B.4 delineate the percentage of the record identified as invalid using the despiking routine discussed above along with the maximum spike duration for each ADV in the random and regular wave cases. These tables indicate the extent to which the despiking was applied at each location. The values given are the maximum from the three components of velocity since the results did not vary by more than a few percent between them.

Table B.1. Percentage of the record identified as invalid and the maximum spike duration for the random wave case at P1-P3. Values are the maximum from the three components of velocity.

Prof.	Distance above bed	A500		A507		A595	
		% Inv.	Max Dur.	% Inv.	Max Dur.	% Inv.	Max Dur.
	[cm]	[%]	[s]	[%]	[s]	[%]	[s]
1	1.2	2	0.42	3	0.74	2	0.44
1	5.3	3	0.50	3	0.80	3	0.64
1	10.2	3	0.42	3	0.52	2	0.56
1	38.0	3	0.36	2	0.32	2	0.32
1	66.0	2	0.48	2	0.30	2	0.32
1	94.0	3	0.50	3	0.54	3	0.48
1	122.0	4	0.44	4	0.64	5	0.56
1	140.0	5	1.30	5	1.24	5	1.28
2	1.1	1	0.34	2	0.38	1	0.26
2	5.2	2	0.40	2	0.38	1	0.26
2	10.2	2	0.38	2	0.40	1	0.30
2	32.0	2	0.28	2	0.40	2	0.22
2	54.0	3	0.34	2	0.44	2	0.44
2	76.0	4	1.66	4	1.42	5	1.12
2	98.0	5	1.28	5	0.70	6	0.56
2	115.0	5	1.32	6	1.54	6	1.36
3	1.1	4	1.22	6	0.62	32	2.72
3	5.1	3	1.06	3	0.94	3	1.92
3	10.2	4	1.18	3	0.70	3	0.46
3	17.2	4	1.22	3	1.62	3	1.92
3	24.0	5	1.24	3	0.62	2	0.42
3	31.0	5	1.98	3	1.78	2	1.08
3	38.0	4	2.02	3	1.52	3	1.40
3	45.0	4	1.76	3	1.04	3	1.72

Table B.2. Percentage of the record identified as invalid and the maximum spike duration for the random wave case at P4-P7. Values are the maximum from the three components of velocity.

Prof.	Distance above bed	A500		A507		A595	
		% Inv.	Max Dur.	% Inv.	Max Dur.	% Inv.	Max Dur.
	[cm]	[%]	[s]	[%]	[s]	[%]	[s]
4	1.2	5	1.80	5	1.72	5	1.50
4	5.2	4	1.20	4	2.22	4	1.32
4	10.2	4	2.00	4	1.56	4	2.22
4	16.2	5	1.54	5	2.06	4	2.30
4	22.0	6	2.26	5	1.50	4	1.48
4	28.0	7	3.18	5	3.60	6	2.12
4	34.0	6	3.78	7	2.82	6	3.12
4	40.0	7	2.76	6	2.42	7	2.70
5	1.1	2	0.88	2	0.38	2	0.66
5	5.1	2	1.26	2	0.58	2	1.36
5	10.0	2	0.82	2	0.54	2	0.46
5	21.0	3	1.18	2	2.52	3	1.32
5	32.0	4	1.76	3	2.22	4	1.64
5	43.0	4	2.28	5	1.64	5	2.14
5	54.0	6	2.24	6	2.26	6	3.24
5	65.0	9	1.90	11	3.18	11	2.20
6	1.2	1	0.24	1	0.32	2	0.38
6	5.1	2	0.32	2	0.24	2	0.60
6	10.1	1	0.40	2	0.30	2	0.52
6	24.0	2	0.30	2	0.42	2	0.46
6	38.0	2	0.76	2	0.62	2	0.58
6	52.0	3	0.46	2	0.42	2	0.60
6	62.0	3	0.64	2	2.30	2	1.04
6	75.0	3	0.62	3	1.26	3	1.58
7	1.2	1	0.34	1	0.64	1	0.32
7	5.0	2	0.68	2	0.58	2	0.36
7	10.1	2	1.04	2	0.72	2	0.36
7	19.0	1	1.68	2	0.62	2	0.98
7	28.0	2	2.72	2	1.74	2	0.54
7	37.0	3	1.78	3	1.28	3	0.64
7	46.0	3	0.52	3	1.08	3	0.50
7	55.0	3	0.44	3	0.52	4	0.96

Table B.3. Percentage of the record identified as invalid and the maximum spike duration for the regular wave case at P1-P3. Values are the maximum from the three components of velocity.

Prof.	Distance above bed	A500		A507	
		% Inv.	Max Dur.	% Inv.	Max Dur.
	[cm]	[%]	[s]	[%]	[s]
1	1.2	1	0.24	3	0.32
1	5.2	1	0.14	2	0.34
1	9.8	1	0.16	2	0.36
1	38.0	1	0.32	1	0.36
1	66.0	1	0.28	1	0.22
1	94.0	2	0.26	2	0.44
1	120.0	4	0.44	5	0.58
1	140.0	8	0.68	11	1.22
2	1.2	0	0.18	1	0.14
2	5.0	1	0.20	1	0.20
2	9.8	1	0.22	1	0.36
2	32.0	1	0.14	1	0.14
2	54.0	1	0.20	1	0.24
2	79.0	4	0.36	5	0.38
2	98.0	5	0.32	5	0.30
2	120.0	6	0.36	7	0.42
3	1.7	16	0.28	40	0.74
3	5.1	1	0.32	3	0.20
3	10.1	1	0.24	3	0.22
3	17.3	1	0.22	3	0.24
3	24.0	1	0.28	3	0.30
3	31.0	11	0.28	13	0.28
3	38.0	6	0.62	9	0.40
3	45.0	5	0.38	9	0.52

Table B.4. Percentage of the record identified as invalid and the maximum spike duration for the regular wave case at P4-P7. Values are the maximum from the three components of velocity.

Prof.	Distance above bed	A500		A507	
		% Inv.	Max Dur.	% Inv.	Max Dur.
	[cm]	[%]	[s]	[%]	[s]
4	1.2	15	0.88	15	1.08
4	5.3	3	0.54	5	0.8
4	10.2	4	0.84	6	1.16
4	16	7	1.36	10	1.3
4	22	10	1.72	14	1.64
4	28	11	1.62	17	2.06
4	34	16	2.34	23	2.1
4	40	20	2.44	32	2.2
5	2.7	2	0.5	6	0.64
5	4.8	1	0.34	3	0.32
5	10.4	2	0.36	5	0.92
5	21	5	1.62	5	1.96
5	32	5	1.38	8	2.96
5	43	7	2.16	13	2.36
5	54	13	1.6	21	1.7
5	65	25	1.8	32	2.12
6	1.1	2	0.22	2	0.26
6	5.1	1	0.2	2	0.26
6	10.1	1	0.24	1	0.2
6	23	1	0.2	1	0.18
6	36	1	0.4	1	0.22
6	49	1	0.32	2	0.32
6	62	2	1.22	1	0.58
6	75	4	1.38	3	0.74
7	1.1	2	0.5	2	0.32
7	5.1	2	0.22	1	0.24
7	10	1	0.22	1	0.2
7	18.9	1	0.26	1	0.24
7	28	2	0.28	2	0.32
7	37	2	0.32	2	0.24
7	46	3	0.28	2	0.42
7	55	4	0.28	3	0.32

B.2.2 Doppler Noise

Figure B.6 illustrates how the noise contribution to the velocity variance from Doppler noise was accounted for in estimates of $\overline{k}$. As discussed in Section 2.5.2, Doppler noise is white noise present at all frequencies and is inherent in all coherent Doppler velocimeter measurements. The magnitude of the Doppler noise is constant at all frequencies and was estimated from the noise floor (flat portion of the spectrum) present at high frequencies (Figure B.6). The magnitude of the noise floor was integrated across the frequency range used to estimate the variance and subtracted from the total variance prior to computing time-averaged turbulent quantities.

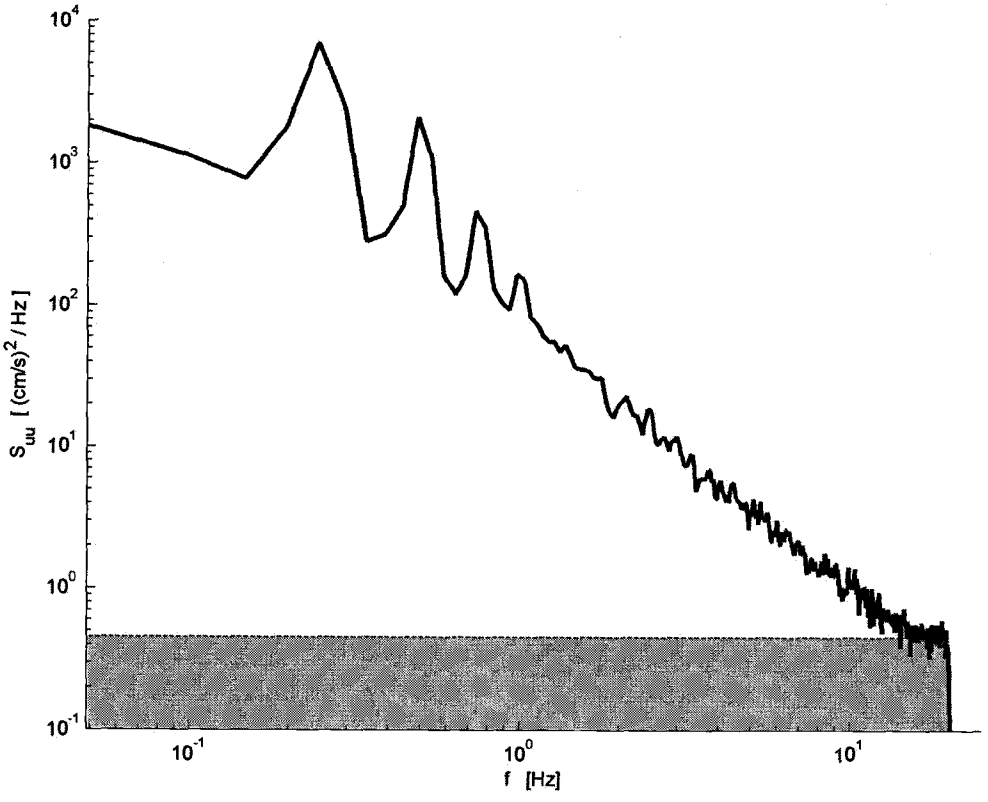

Figure B.6. Despiked cross-shore velocity spectrum for the regular wave case at P4, 34 cm above the bed. Data are from ADV A500 and have been filtered to remove instrument vibration. The Doppler noise contribution to the variance is shown by the shaded region.

B.2.3 Instrument Vibration

Figures B.7 and B.8 illustrate the high frequency instrument vibration discussed in Section 2.5.2. As the waves hit the 40 cm stem on the ADV, it vibrated horizontally and created a peak in the energy near 24 Hz in both the *u* and *v* components of velocity (Figures B.7 and B.8). The waves also hit the supports used to deploy the ADVs, shown in Figures A.5 and A.6. These supports were much more rigid in the cross-shore than the alongshore direction, and as a result, the vibration of the supports only appeared in the *v* component of velocity at frequencies between 12 – 20 Hz (Figure B.8). The noise contribution due to this instrument vibration was removed by low-pass filtering the data, shown by the dashed line in Figures B.7 and B.8. Details of the filters used are provided in Section 2.5.2.

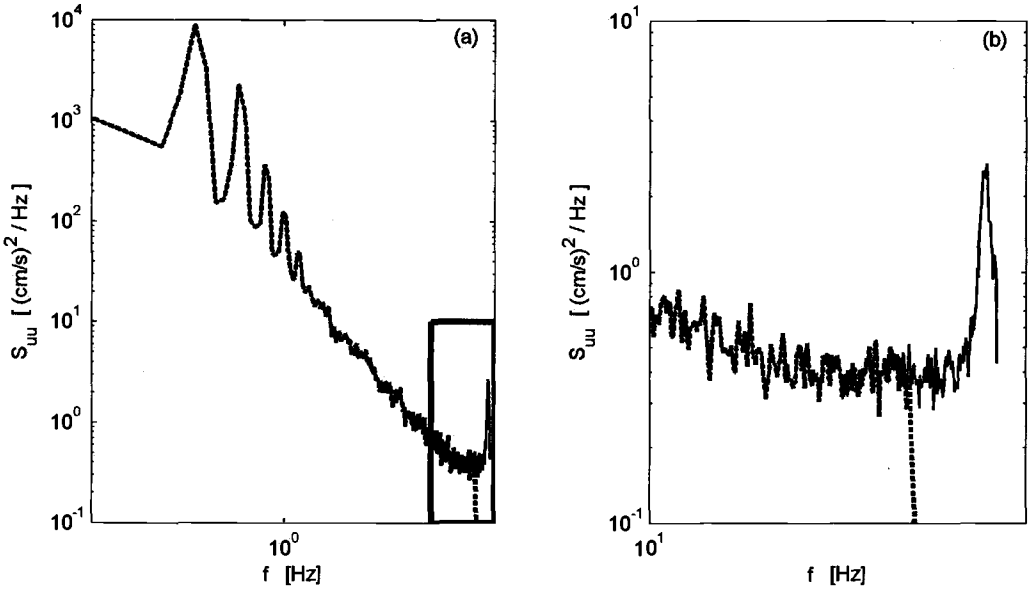

Figure B.7. Despiked (solid) and filtered (dash) cross-shore velocity spectra. Noise due to vibration of the 40 cm stem on the ADV shown at 24 Hz in (a) and magnified in (b). Data are from ADV A500 at P4, 5.3 cm above the bed in the regular wave case.

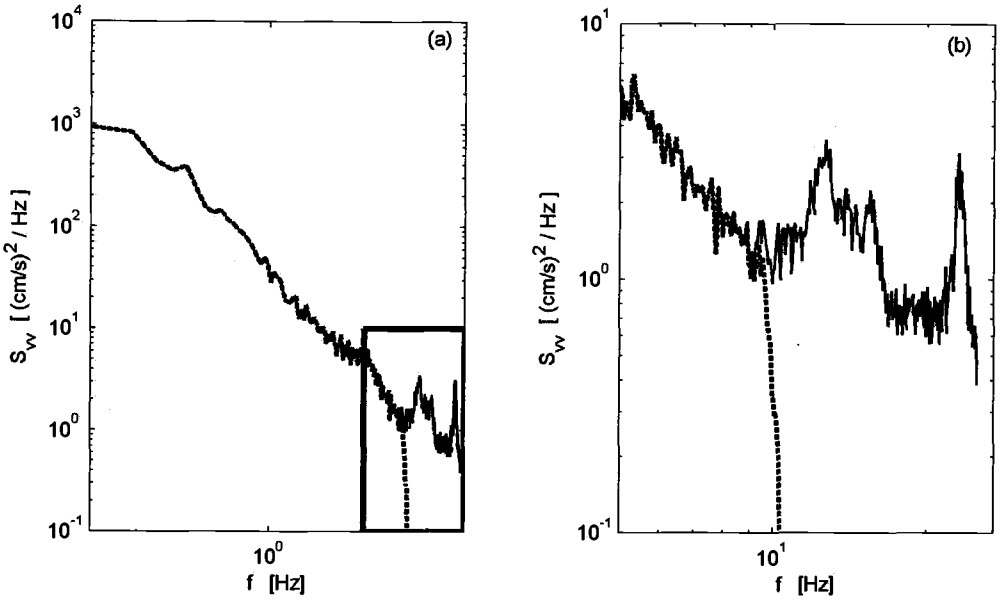

Figure B.8. Despiked (solid) and filtered (dash) alongshore velocity spectra. Noise due to vibration of the 40 cm stem on the ADV shown at 24 Hz, and noise due to vibration of the ADV supports shown between 12 Hz - 20 Hz in (a) and magnified in (b). Data are from ADV A500 at P4, 5.3 cm above the bed in the regular wave case.

Appendix C. Example Applications of the Turbulence Separation Methods

The following sections illustrate the application of each of the three methods used to separate the turbulent and wave-induced components of velocity in both the time and frequency domains. Examples are shown for all three components of velocity because in other sections the cross-shore component is typically shown and these examples provide the reader with a glimpse of time series and spectra from the other two components of velocity. A description of each method along with the details regarding their application can be found in Sections 2.3 and 2.6, respectively.

C.1 Ensemble Averaging

Figures C.1 - C.3 illustrate the application of the ensemble averaging method to all three components of velocity for the regular wave case at P6, 62 cm above the bed (near trough level). Data are from ADV A500 and were high-pass filtered to remove low-frequency motions prior to applying the ensemble averaging technique, which is discussed in further detail below. In the time domain, the wave-induced component of velocity was the portion of the record repeated over approximately one wave period and the turbulent component was the difference between the total and wave-induced components. This was clear in the cross-shore (Figures C.1a and C.1b) and vertical (Figures C.3a and C.3b) components of velocity. However, because the waves were alongshore uniform, the wave-induced component had little meaning in the alongshore direction and the turbulent component resembled the total velocity (Figures C.2a and C.2b). In the frequency domain, energy at the peak wave frequency (0.25 Hz) was

significantly reduced (Figures C.1c – C.3c), providing an excellent indication of the effectiveness of ensemble averaging in removing the wave-induced component of velocity.

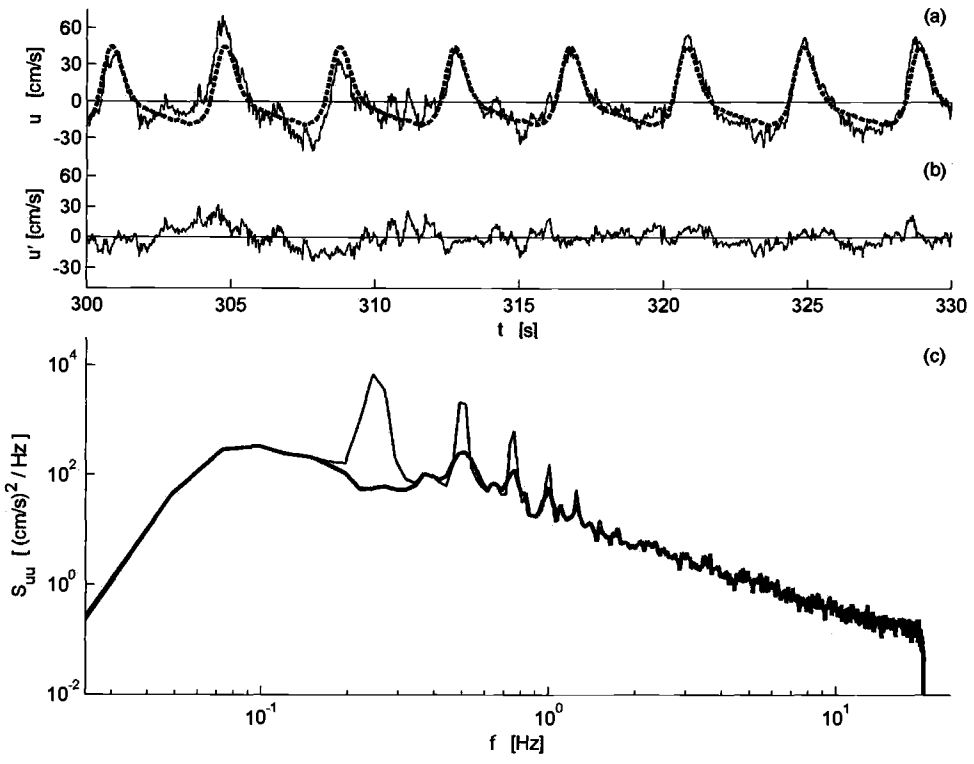

Figure C.1. Application of the ensemble averaging technique to the cross-shore velocity from ADV A500 at P6, 62 cm above the bed in the regular wave case. The time domain contains the total (a, solid), wave-induced (a, dash), and turbulent (b) components of velocity. The frequency domain (c) contains spectra for the total (light) and turbulent (heavy) components of velocity. All data were high-pass filtered to remove low-frequency motions.

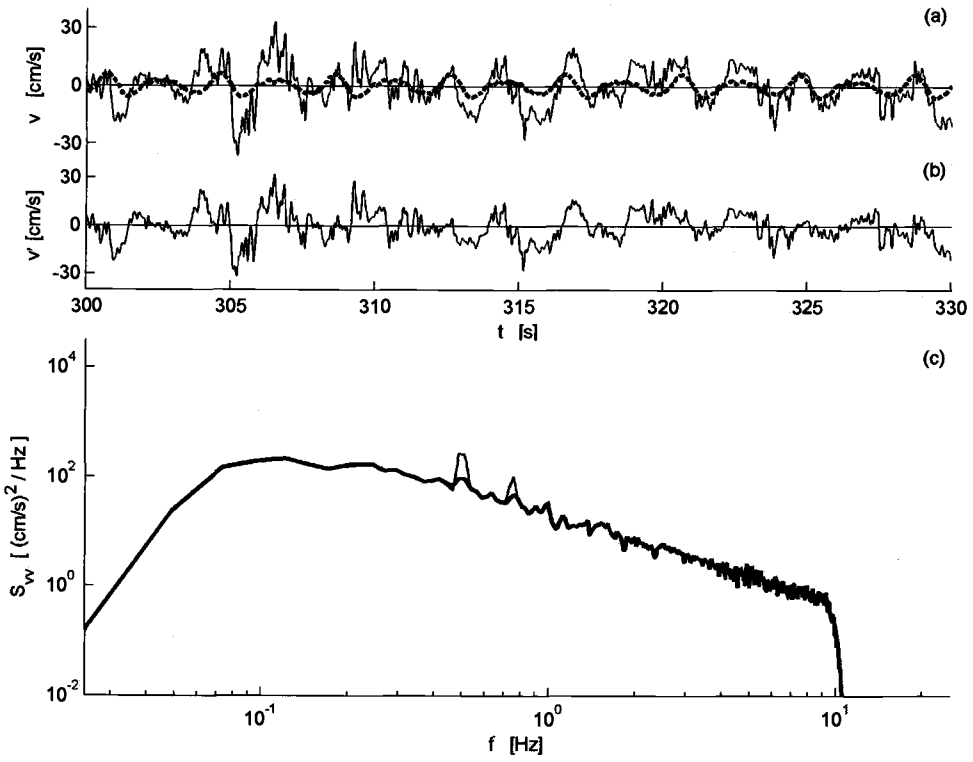

Figure C.2. Application of the ensemble averaging technique to the alongshore velocity from ADV A500 at P6, 62 cm above the bed in the regular wave case. The time domain contains the total (a, solid), wave-induced (a, dash), and turbulent (b) components of velocity. The frequency domain (c) contains spectra for the total (light) and turbulent (heavy) components of velocity. All data were high-pass filtered to remove low-frequency motions.

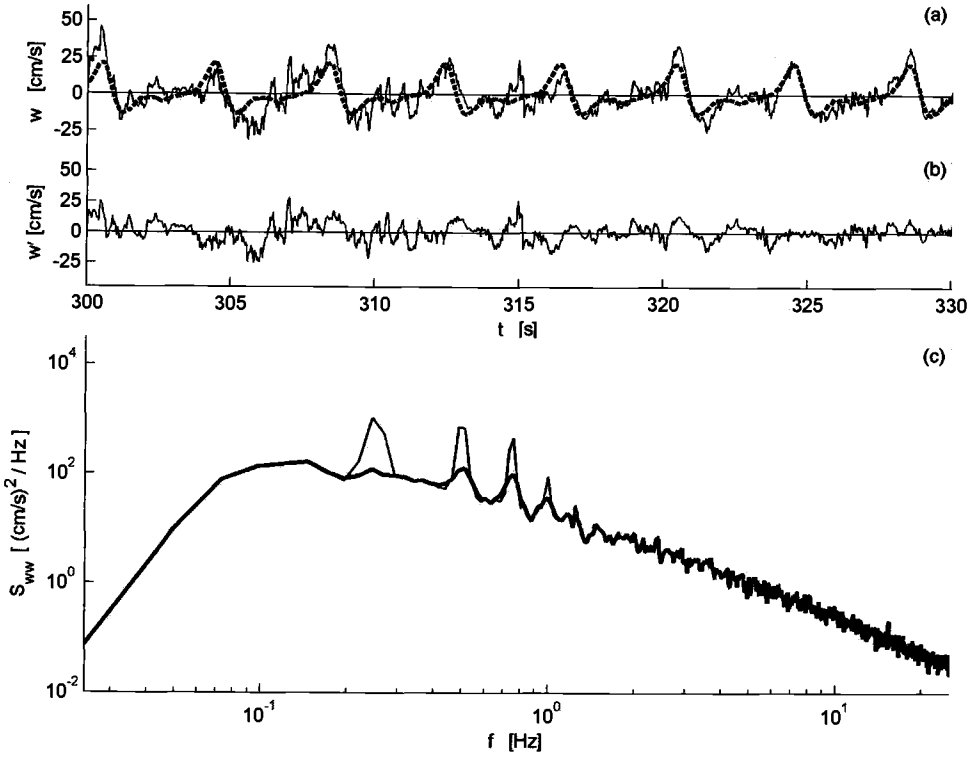

Figure C.3. Application of the ensemble averaging technique to the vertical velocity from ADV A500 at P6, 62 cm above the bed in the regular wave case. The time domain contains the total (a, solid), wave-induced (a, dash), and turbulent (b) components of velocity. The frequency domain (c) contains spectra for the total (light) and turbulent (heavy) components of velocity. All data were high-pass filtered to remove low-frequency motions.

When using the ensemble averaging method, care must be taken to remove low-frequency velocity fluctuations, primarily in the cross-shore component of velocity, prior to computing the turbulent component of velocity. The reason for this is illustrated in Figure C.4. In the upper two panels (Figures C.4a and C.4b), the low-frequency component was not removed from the time series, resulting in an apparent

increase in the magnitude of the turbulent velocity from $t = 315$ s – 330 s when the wave component was subtracted from the total velocity.

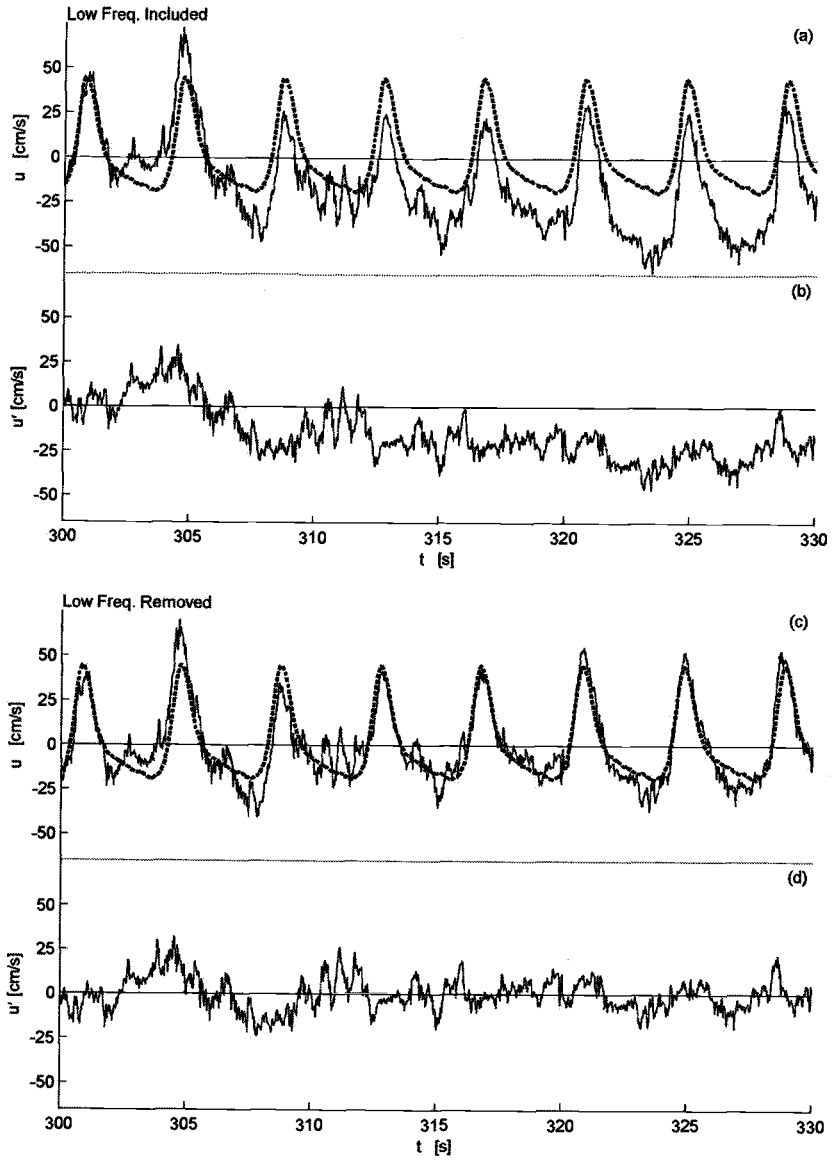

Figure C.4. Illustration of pseudo-turbulence generated by low-frequency fluctuations in the cross-shore velocity. Data are from ADV A500 at P6, 62 cm above the bed in the regular wave case. Data that have not been high-pass filtered are shown in (a) and (b). Panels (c) and (d) are data used in this test, which have been high-pass filtered.

This increase in turbulent energy, or "pseudo-turbulence," is a direct result of the ensemble averaging technique, not physical processes, and was accounted for by high-pass filtering all velocity data at 0.0625 Hz prior to using this technique, as shown in Figures C.4c and C.4d. In doing this we see that the pseudo-turbulence present from $t = 315$ s – 330 s was minimized and a more accurate estimate of the turbulent velocity was obtained.

C.2 High-Pass Filtering

Figures C.5 - C.7 illustrate the application of the high-pass filtering method to isolate the turbulent component of velocity. The data are from ADV A500 at P4, 34 cm above the bed in the random wave case. In this case, the turbulent spectrum does not contain significant energy contributions from the peak wave frequency or its harmonics, indicating that the 1 Hz high-pass filter was effective in removing the wave component of velocity. This is no coincidence since the cutoff frequency was chosen to minimize the amount of pseudo-turbulence caused by energy present in the wave harmonics. However, this cutoff neglected turbulent energy at frequencies lower than 1 Hz and the turbulent quantities obtained using high-pass filtering were smaller than the other two methods.

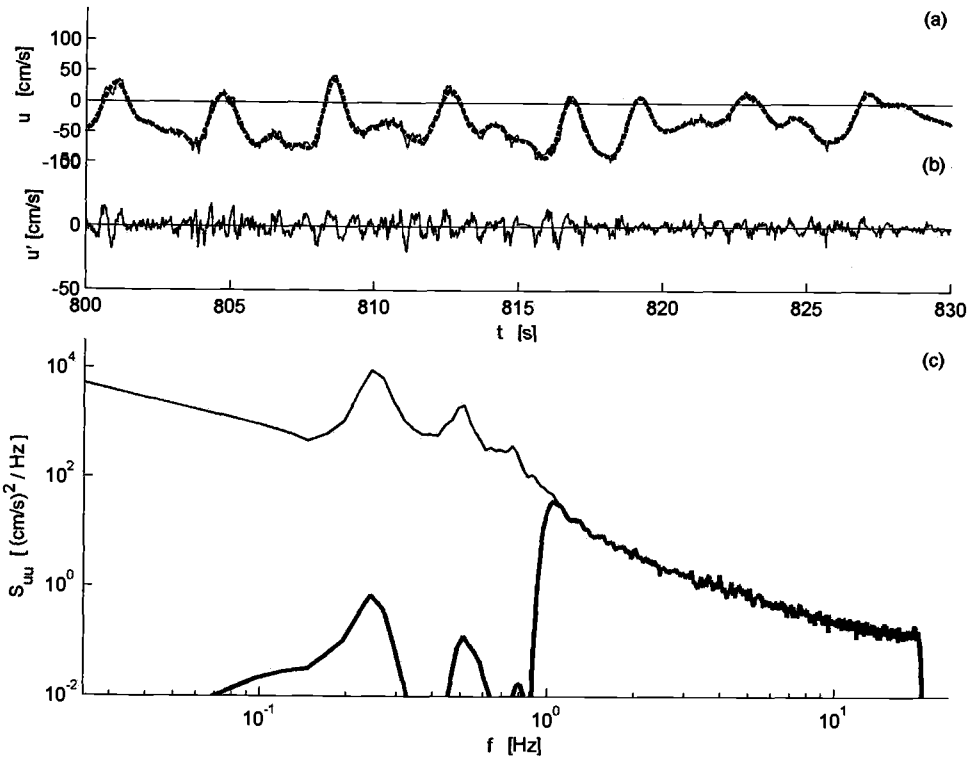

Figure C.5. Application of the high-pass filtering technique to the cross-shore velocity from ADV A500 at P4, 34 cm above the bed in the random wave case. The time domain contains the total (a, light), wave-induced (a, dash), and turbulent (b) components of velocity. The frequency domain (c) contains the total (light) and turbulent (heavy) components of velocity.

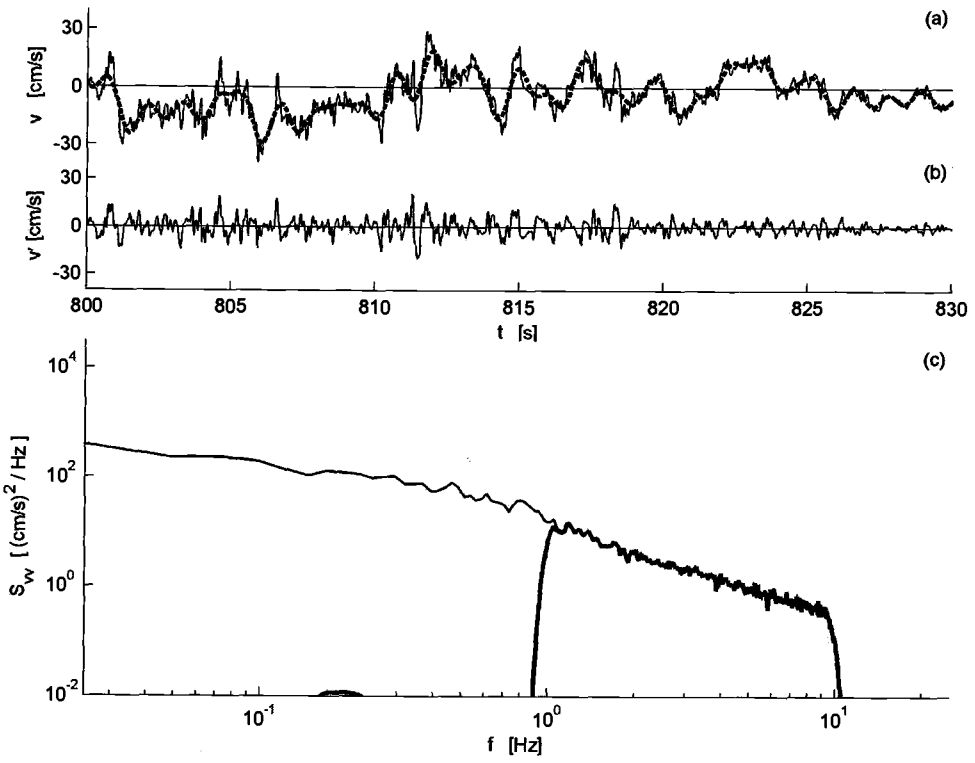

Figure C.6. Application of the high-pass filtering technique to the alongshore velocity from ADV A500 at P4, 34 cm above the bed in the random wave case. The time domain contains the total (a, light), wave-induced (a, dash), and turbulent (b) components of velocity. The frequency domain (c) contains the total (light) and turbulent (heavy) components of velocity.

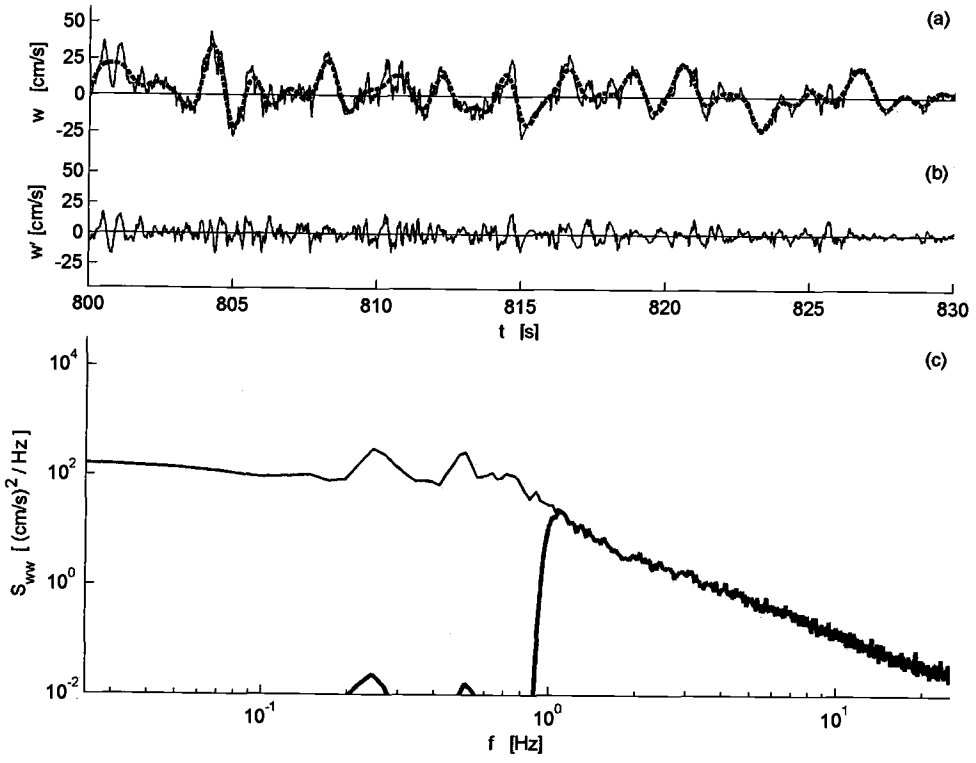

Figure C.7. Application of the high-pass filtering technique to the vertical velocity from ADV A500 at P4, 34 cm above the bed in the random wave case. The time domain contains the total (a, light), wave-induced (a, dash), and turbulent (b) components of velocity. The frequency domain (c) contains the total (light) and turbulent (heavy) components of velocity.

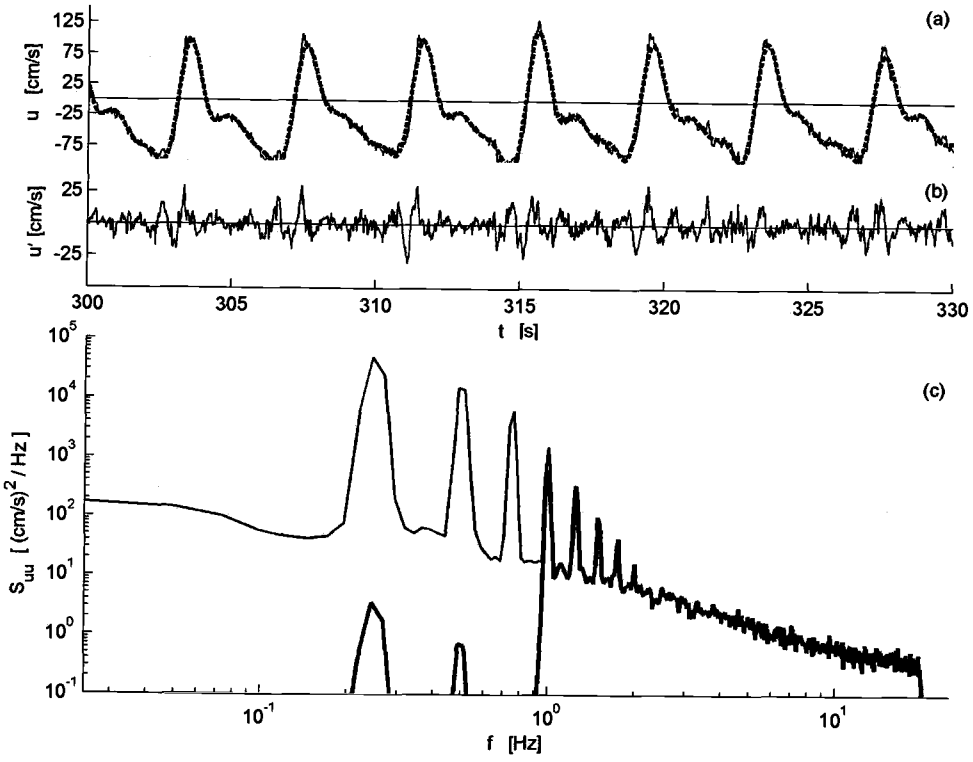

Figure C.8. Illustration of pseudo-turbulence generated by wave energy at harmonics higher than the 1 Hz cutoff frequency. Data are the cross-shore velocity from ADV A500 at P3, 38 cm above the bed in the regular wave case.

In Figures C.5 – C.7 there appeared to be little wave energy at frequencies greater than 1 Hz, indicating that the high-pass filter effectively removed the wave energy from the total velocity. However, examining the cross-shore turbulent spectrum from ADV A500 at P3, 38 cm above the bed in the regular wave case (Figure C.8c), it is clear that this cutoff was not successful in eliminating energy present at higher wave harmonics in every case. This highlights the problem associated with this method. At breaking, where the waves were highly non-linear and the turbulent velocities were large, the overlap in scales between the waves and turbulence eliminated the possibility of

specifying a single cutoff frequency to separate the two. A low cutoff would bias the turbulent energy high by including energy from the wave harmonics; however, a high cutoff would bias the turbulent energy low by neglecting contributions from low-frequency vortices.

C.3 Differencing

Figures C.9 – C.11 illustrate the application of Trowbridge's (1998) differencing method to the measured velocities from ADVs A500 (u_1) and A507 (u_2) at P4, 34 cm above the bed in the random wave case. The upper panel (a) shows a portion of the total velocity time series from each ADV, followed by the difference in the middle panel (b), given by:

$$\Delta u = u_1 - u_2 \tag{C.1}$$

The lower panel (c) contains the velocity spectra from u_1, u_2, and $\frac{1}{2}\Delta u$. The power spectral density for Δu was divided by 2 per Eq. 2.3 and represents the average turbulent energy between the ADVs. In the frequency domain (Figures C.9c – C.11c), the wave energy was significantly reduced, indicating that this method effectively separated the wave-induced and turbulent components of velocity.

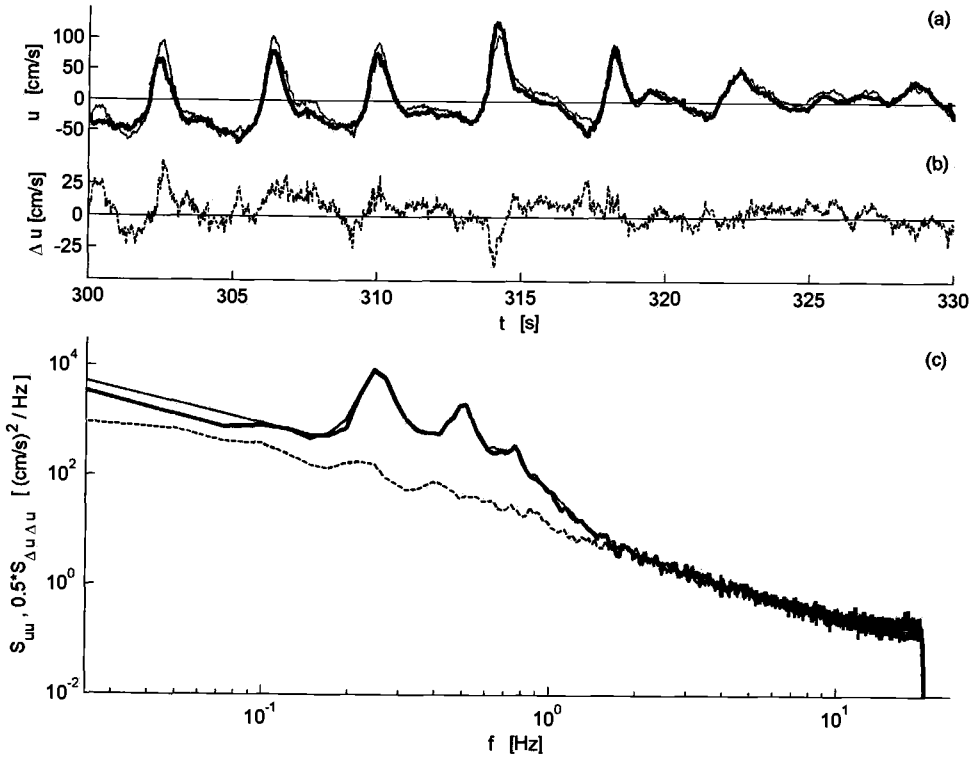

Figure C.9. Application of the differencing technique to the cross-shore velocity at P4, 34 cm above the bed in the random wave case. Data are from ADVs A500 (light), A507 (heavy), and the difference between A500 and A507 (dash).

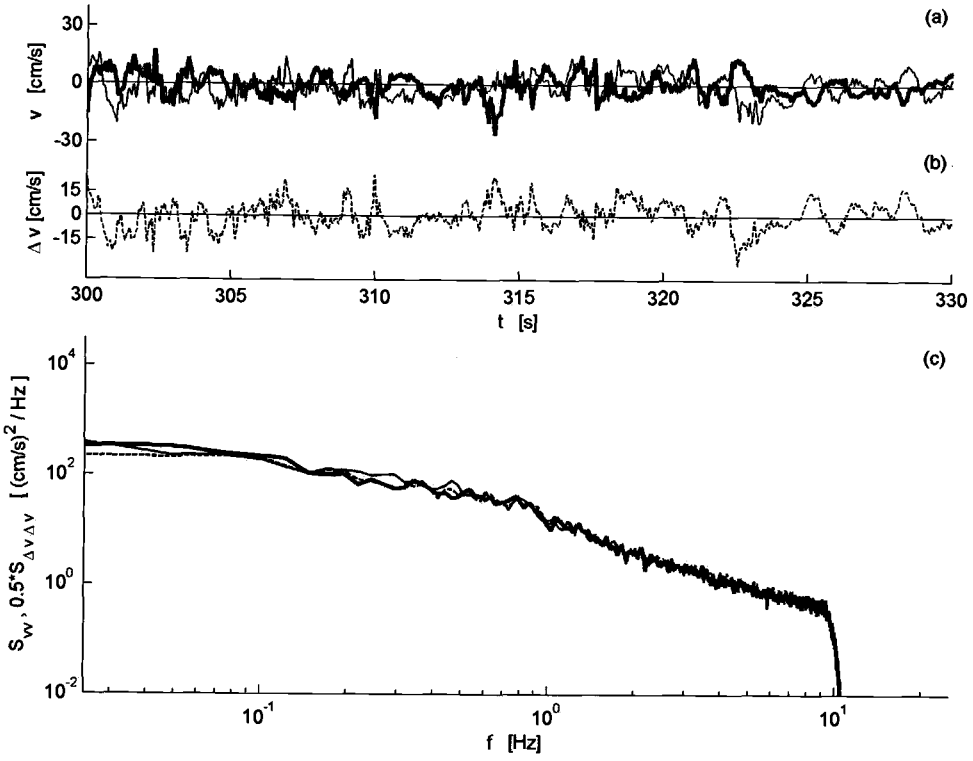

Figure C.10. Application of the differencing technique to the alongshore velocity at P4, 34 cm above the bed in the random wave case. Data are from ADVs A500 (light), A507 (heavy), and the difference between A500 and A507 (dash).

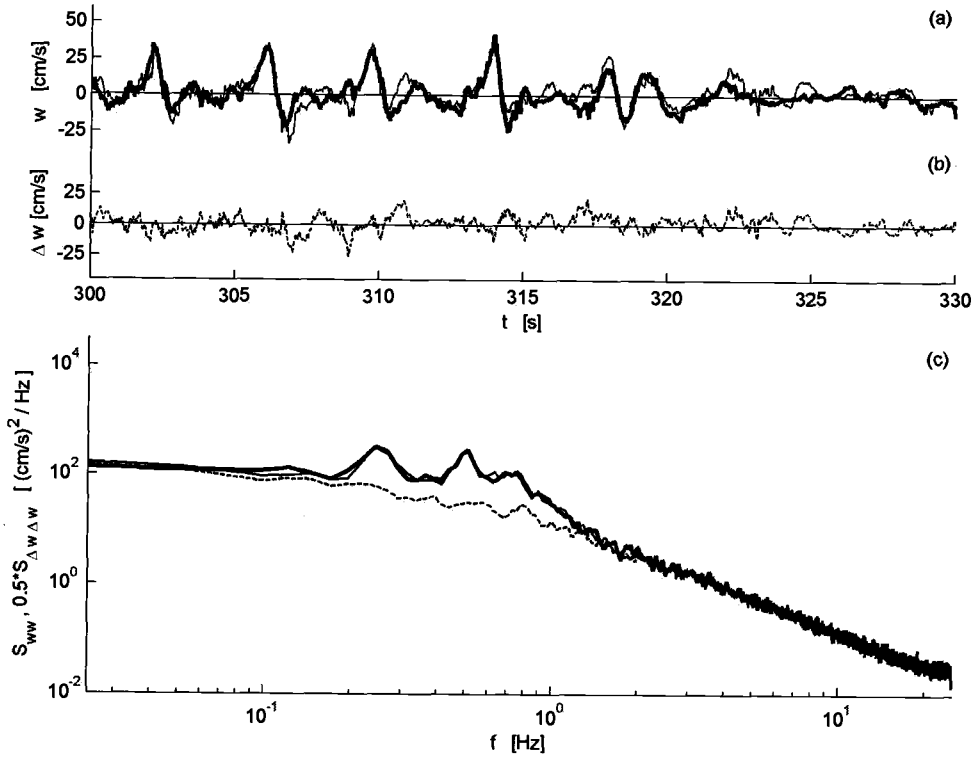

Figure C.11. Application of the differencing technique to the vertical velocity at P4, 34 cm above the bed in the random wave case. Data are from ADVs A500 (light), A507 (heavy), and the difference between A500 and A507 (dash).

In the regular wave case, the bias in the differencing estimates at P7 (Section 2.6), was due to an alongshore partial standing wave and is illustrated in Figures C.12 and C.13. The data in these figures are from ADVs A500 and A507 near the trough level (55 cm above the bed) of non-breaking waves; therefore, very little turbulent energy is expected. Figure C.12b indicates that there was turbulent energy present; however, it is clear from the upper panel (Figure C.12a) that this pseudo-turbulence is a direct result of the differencing technique. The non-zero alongshore component of velocity (Figure C.13) confirms that the alongshore partial standing wave created a component

of velocity parallel to the sensor separation and violated the assumption that each sensor recorded the same wave-induced component of velocity. This was the only location affected by this standing wave and did not influence our conclusions due to the lack of turbulent energy observed at P7.

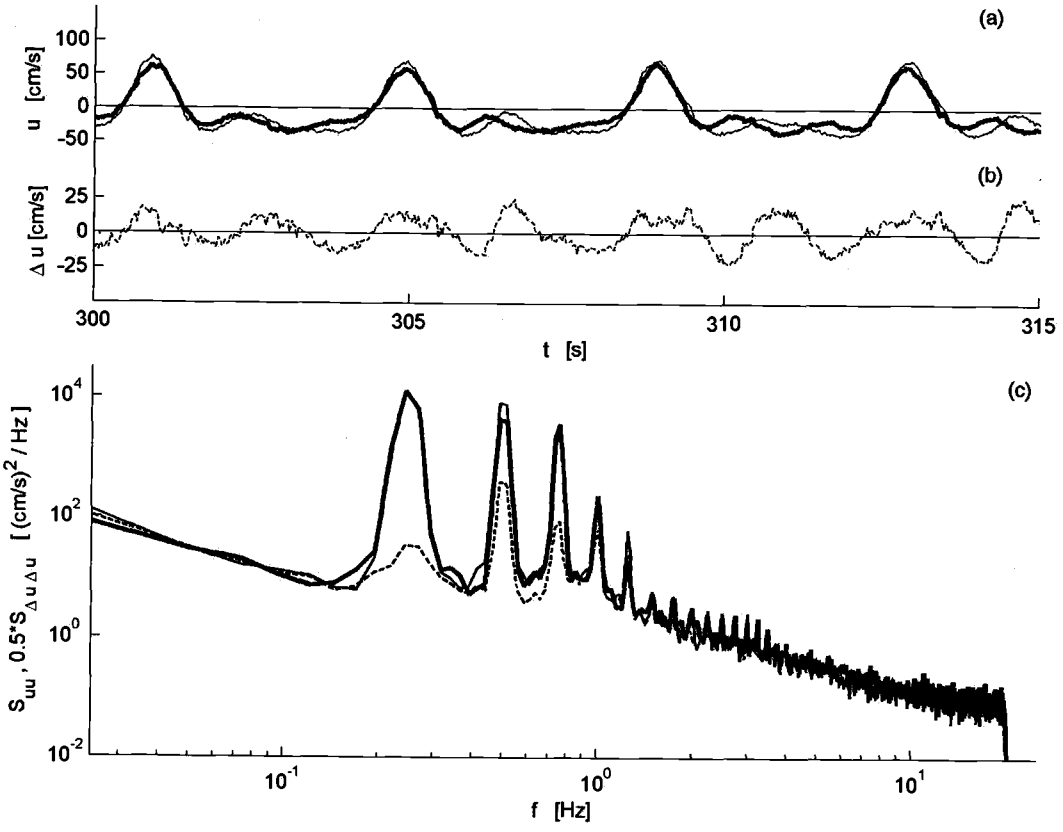

Figure C.12. Illustration of pseudo-turbulence generated by the alongshore partial standing wave when using the differencing technique. Data are the cross-shore velocity at P7, 55 cm above the bed in the regular wave case from ADVs A500 (light), A507 (heavy), and the difference between A500 and A507 (dash).

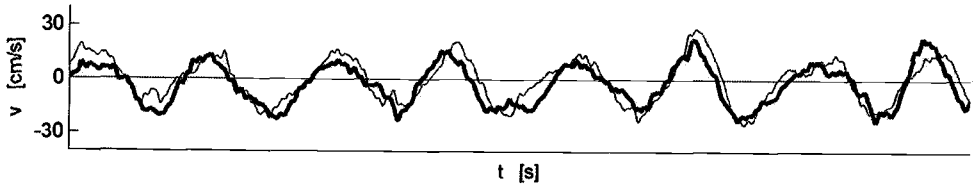

Figure C.13. Alongshore velocity at P7, 55 cm above the bed in the regular wave case. Data are from ADVs A500 (light) and A507 (heavy).

Appendix D. Alongshore Variation in Turbulence over the Bar

This section provides additional detail regarding the alongshore variation of $\bar{k}$, or the variation among the three ADVs aligned parallel with the wave crest. Throughout Section 2, the average value of $\bar{k}$ was calculated using estimates from all of the ADVs in the array. It is useful to examine how $\bar{k}$ varied in the alongshore direction (parallel to the wave crests) to determine if the average value of $\bar{k}$ was biased by alongshore variations at each measurement location.

Figures D.1 and D.2 show the variation between all three ADVs in the random wave case at all 7 profiles using estimates from the high-pass filtering and differencing methods. The high-pass filtering estimates (Figure D.1) showed little alongshore variation at every location, with the exception of P3 (Figure D.1c), indicating that the average value reported in Section 2 was not biased by alongshore variations in the turbulence.

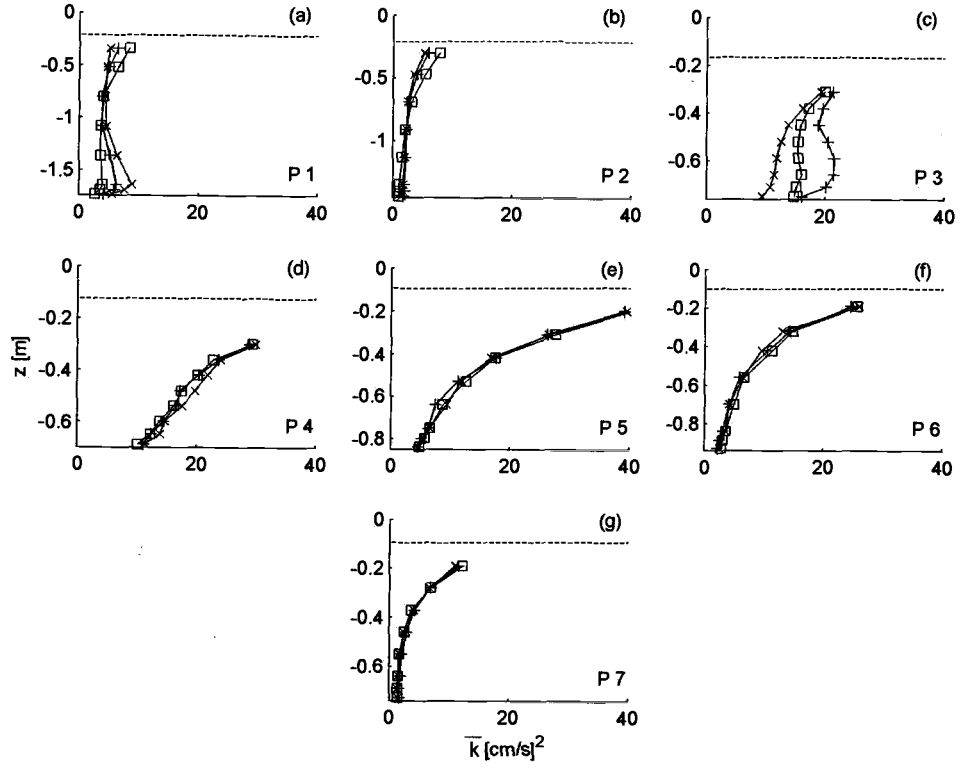

Figure D.1. Alongshore variation of $\bar{k}$ computed using the high-pass filtering method in the random wave case for profiles 1-7 (a-f). Data from ADVs A500 (x), A507 (+), and A595 (□) are shown. Trough level indicated by (--), bottom of the figure indicates the fixed bed.

The differencing estimates (Figure D.2) exhibited a similar trend. It is important to note that we expect estimates of $\bar{k}$ to decrease as the spacing between the sensors decreases because the turbulence between the sensors will become correlated and recorded as wave induced motion. This explains why in almost every case, the estimates from the difference of ADVs A507 and A595 (smallest spacing) were slightly less than estimates from the other two ADV pairs.

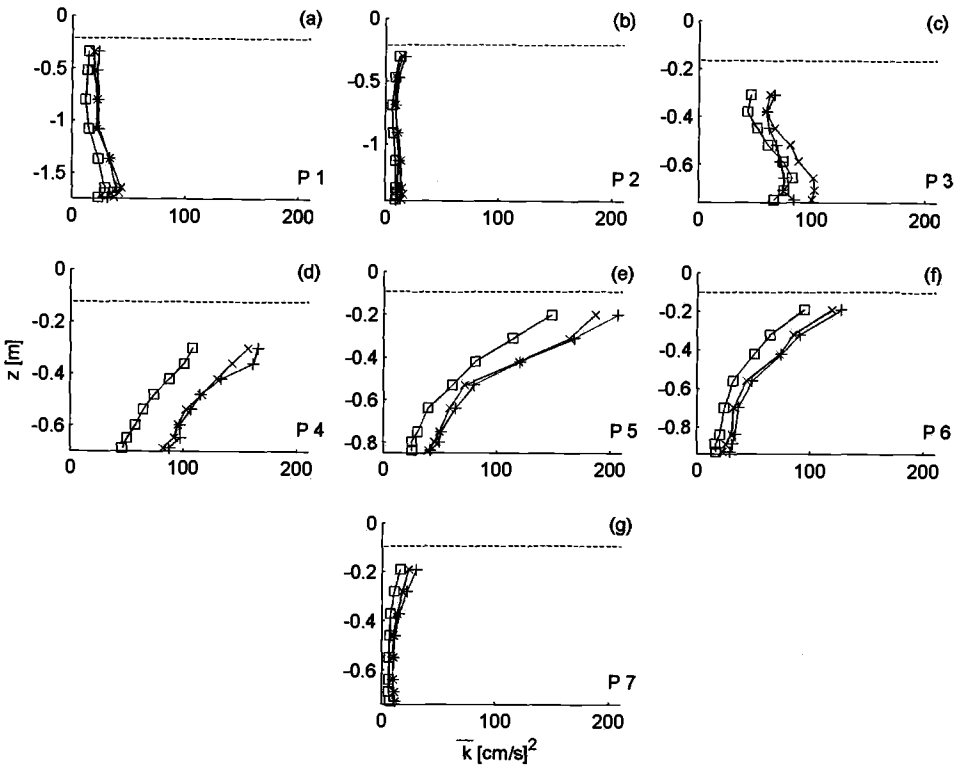

Figure D.2. Alongshore variation of $\bar{k}$ computed using the differencing method in the random wave case for profiles 1-7 (a-f). Data are from the difference of ADVs A500 and A507 (x), A500 and A595 (+), and A507 and A595 (□). Trough level indicated by (--), bottom of the figure indicates the fixed bed.

Figures D.3 and D.4 illustrate the alongshore variation in the regular wave case at all 7 profile locations using estimates from the ensemble averaging and high-pass filtering methods obtained using ADVs A500 and A507. The differencing method was not included because only two ADVs were used in the regular wave case (refer to Section 2.4.3), resulting in a single differencing estimate. As in the random wave case, there was little deviation in the alongshore direction at every measurement location, with the exception of P3. The reason for the deviation at P3 is unclear, but the fact that it was

observed using two different separation techniques indicates that it was not a product of the method used to separate the wave-induced and turbulent components of velocity.

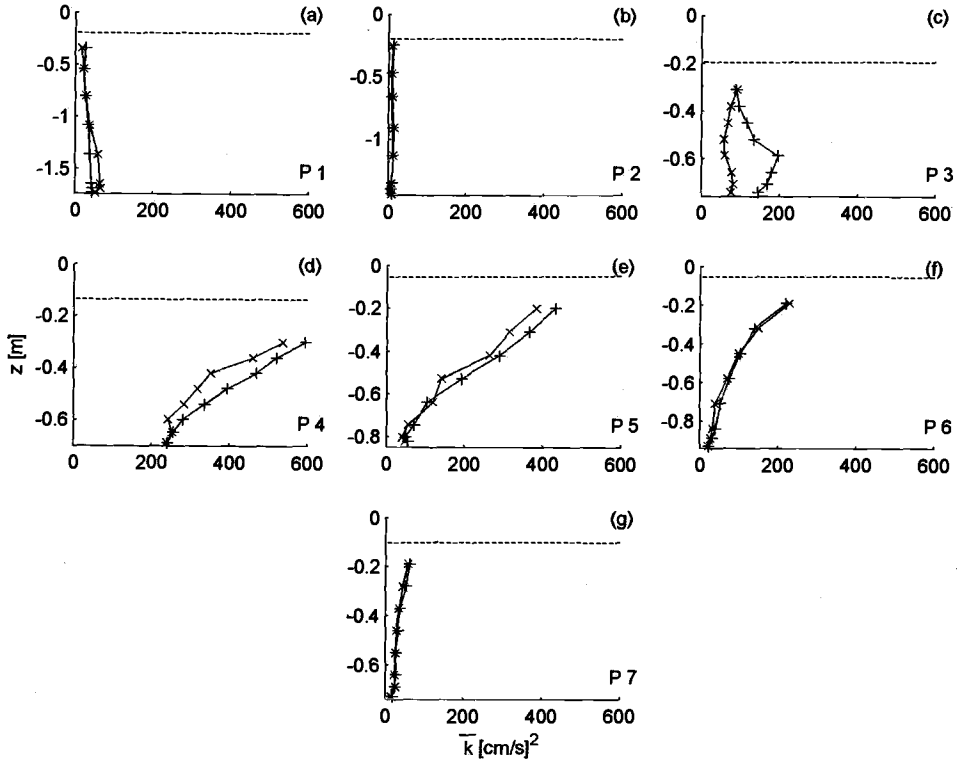

Figure D.3. Alongshore variation of $\overline{k}$ computed using the ensemble averaging method in the regular wave case for profiles 1-7 (a-f). Data from ADV A500 (x) and A507 (+) are shown. Trough level indicated by (--), bottom of the figure indicates the fixed bed.

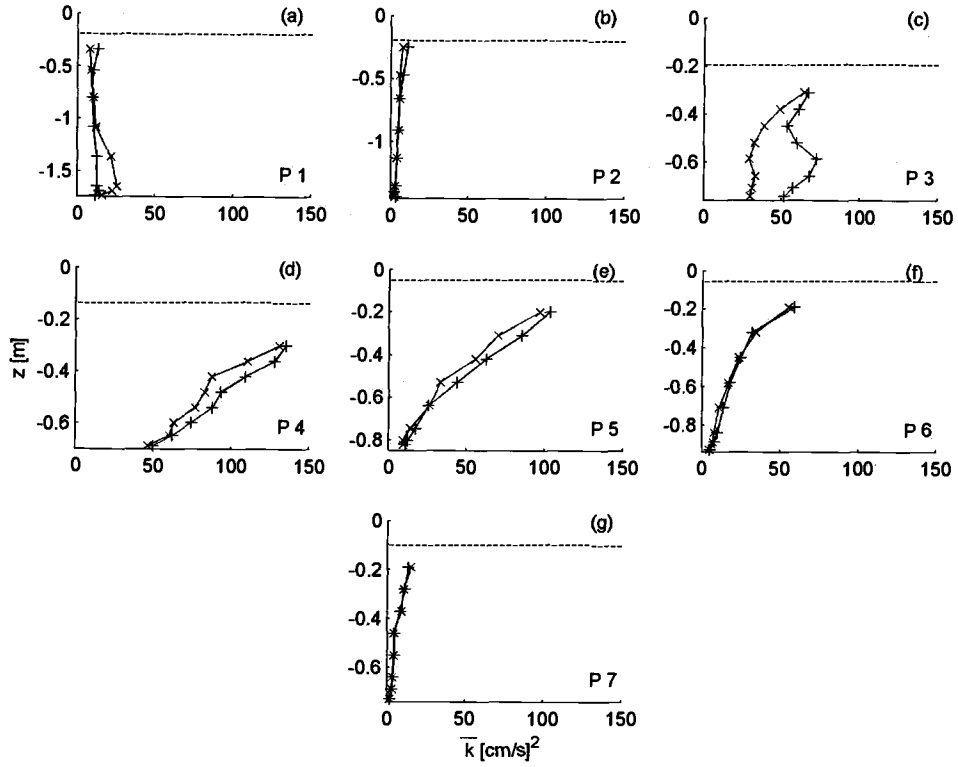

Figure D.4. Alongshore variation of $\overline{k}$ computed using the high-pass filtering method in the regular wave case for profiles 1-7 (a-f). Data from ADV A500 (x) and A507 (+) are shown. Trough level indicated by (--), bottom of the figure indicates the fixed bed.

Taken as a whole, Figures D.1 – D.4 indicate that the average value of $\overline{k}$ reported in Section 2 was not biased by variations in the alongshore direction and accurately reflects the average turbulent energy within the water column.

Appendix E. Correlation of Wave Breaking and Changes in the Mean Flow

This section contains a preliminary investigation into the possibility that periods of intense, sustained wave breaking force changes in the mean flow calculated over timescales of several wave periods. In the random wave case, observations indicated that significant changes in the magnitude and direction of the low-frequency (less than 0.0625 Hz) component of the cross-shore velocity (u_{LF}) were correlated with changes in the turbulent energy within the water column. It is possible that this was due to groups of plunging waves injecting mass into the water column that quickly returned offshore, resulting in an increase in the mean offshore velocity. To investigate this in a qualitative sense, the mass flux was computed by depth integrating u_{LF} (a "slowly varying undertow") to trough level:

$$Q(t) = \int_{-h}^{T.L.} u_{LF}(z,t)dz \tag{E.1}$$

The time-dependent, depth integrated turbulent kinetic energy, k_{int}, was estimated from the high-pass filtered data and provided a proxy for the presence and intensity of wave breaking. This was averaged using a trailing average of 4 wave periods, k_{ta}, to allow time for the mass introduced by breaking to return offshore and compared to Q. All data are the average from the 3 ADVs used in the random wave test.

$$k_{\text{int}}(t) = \int_{-h}^{T.L.} k(z,t)dz \tag{E.2}$$

$$k_{ta}(t_0) = \frac{\Delta t}{4T}\sum_{t_0-4T}^{t_0} k_{\text{int}}(t) \tag{E.3}$$

Figure E.1 illustrates the correlation found between k_{ta} and Q directly over the bar crest (P4). Note that in this figure $-Q$ is plotted (i.e. a positive value indicates an offshore-directed flow) and $-Q$ and k_{ta} are normalized by $-Q_{max}$ and $2(k_{ta})_{max}$, respectively, for plotting. In this figure we see that strong offshore flows correlate with intense and sustained wave breaking events, indicating that wave breaking is not only important in terms of the turbulence generated, but also in forcing changes in the mean flow. Further work is needed to extend these results to other cross-shore locations and include additional terms in the horizontal momentum equation such as the mean water level gradient.

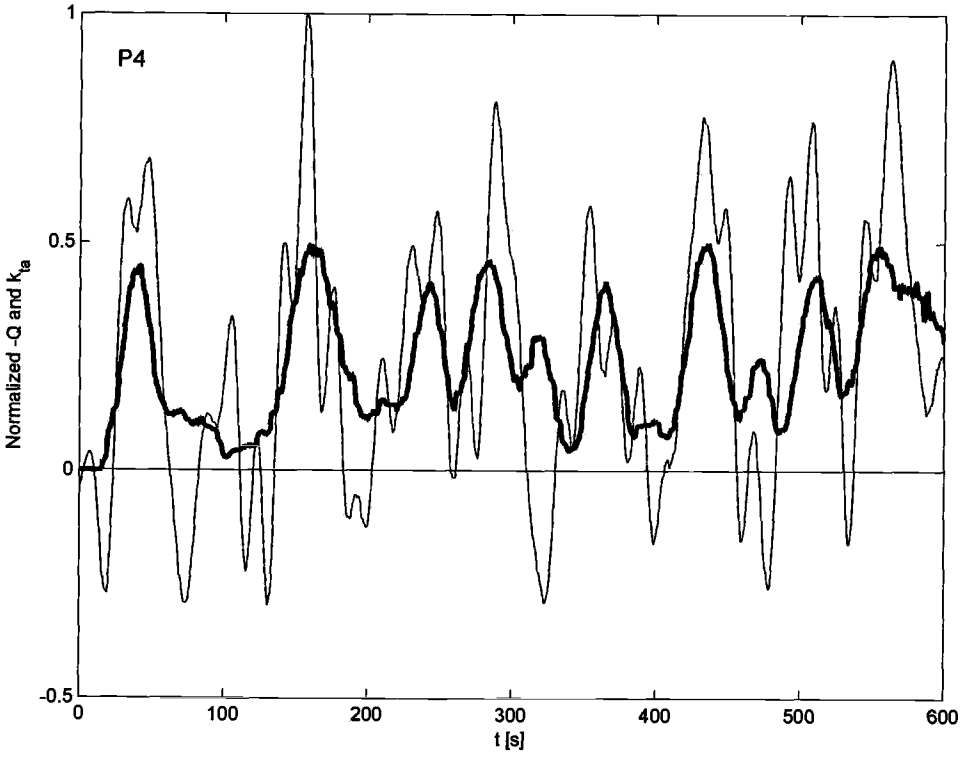

Figure E.1. Time variation of the normalized mass flux below trough level ($-Q$) (light) and the normalized depth integrated turbulent kinetic energy (k_{ta}) (heavy) at the bar crest (P4).

Appendix F. Presentation at ICCE 2004, Lisbon, Portugal

This work was presented at the 29th International Conference on Coastal Engineering (ICCE) in Lisbon, Portugal and published in the proceedings (Scott *et al.* 2004). The conference took place September 19-24, 2004. The presentation was 12 minutes long with additional time for questions and consisted of a total of 32 slides excluding transitional slides, shown in Figures F.1 – F.4.

Travel was funded by the O.H. Hinsdale Wave Research Laboratory under National Science Foundation (NSF) grants. The week long conference was attended by several students from Oregon State University and included a number of interesting talks. During this conference I was able to meet with Dr. Tom Hsu and begin discussing the possibility of collaborating on future research using the data set described in this thesis. This led to the opportunity to attend Woods Hole Oceanographic Institution as a guest graduate student and work with Dr. Hsu in March, 2005.

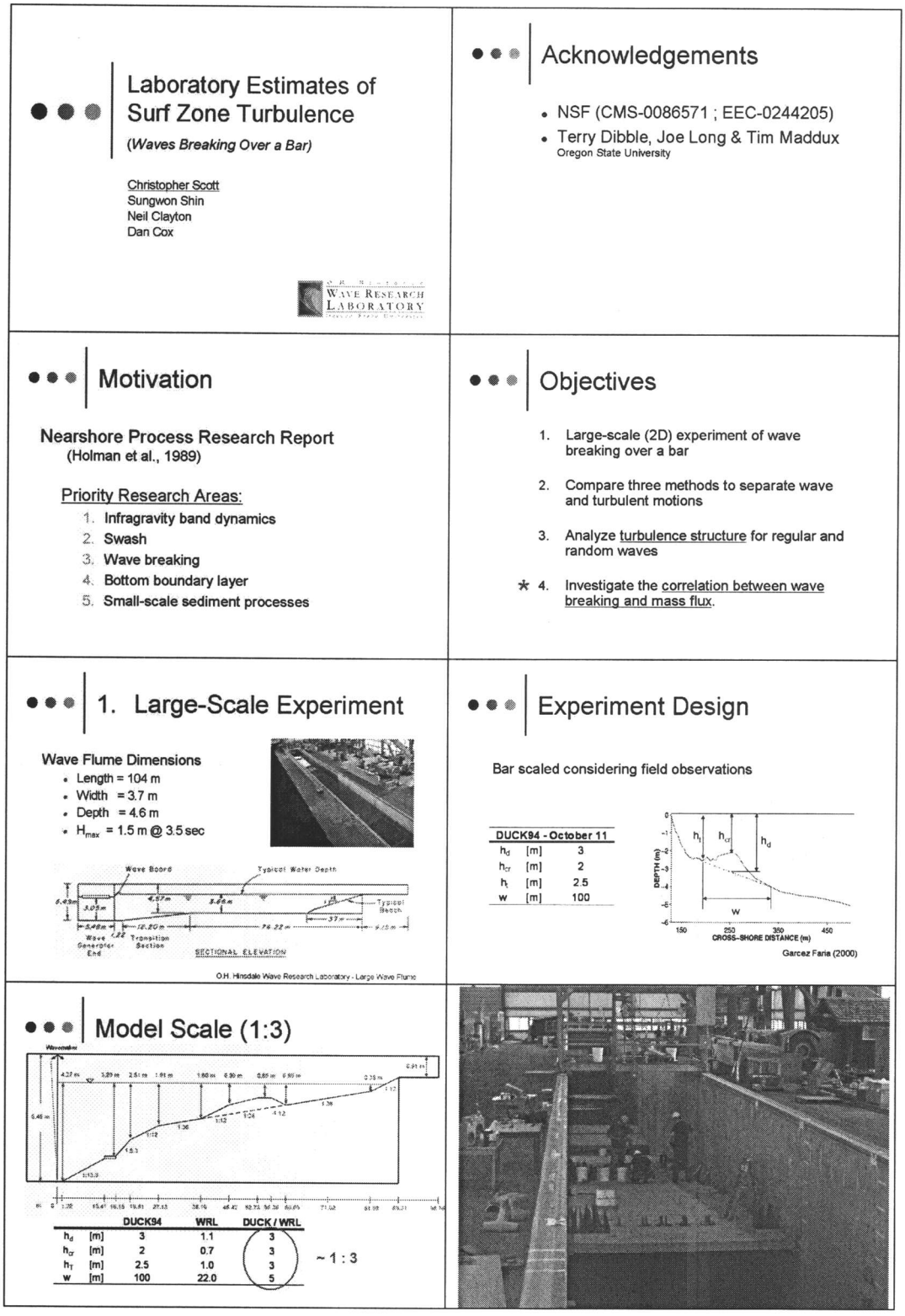

Figure F.1. Slides 1-8 presented at ICCE 2004. Organized left to right, top to bottom.

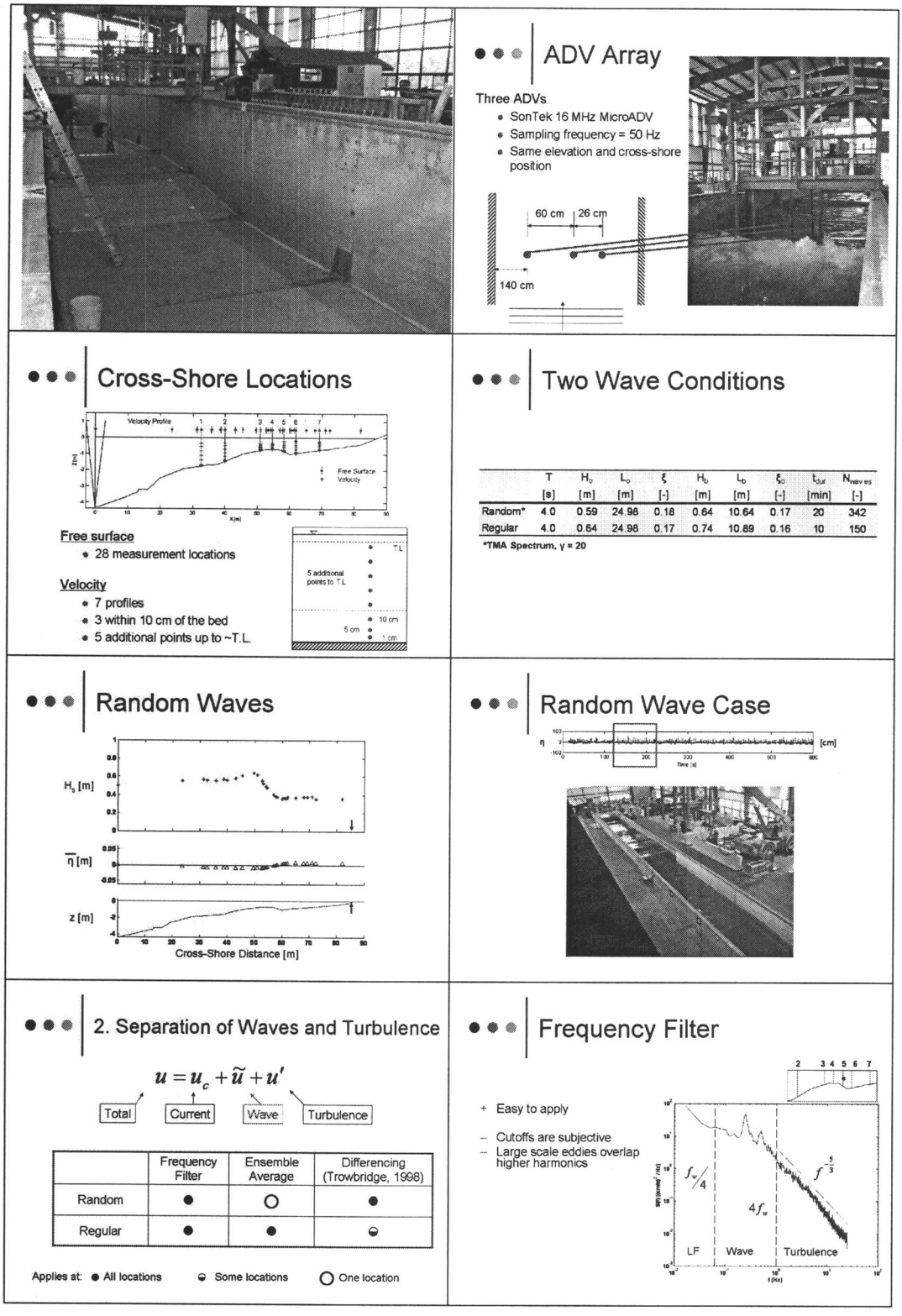

Figure F.2. Slides 9-16 presented at ICCE 2004. Organized left to right, top to bottom.

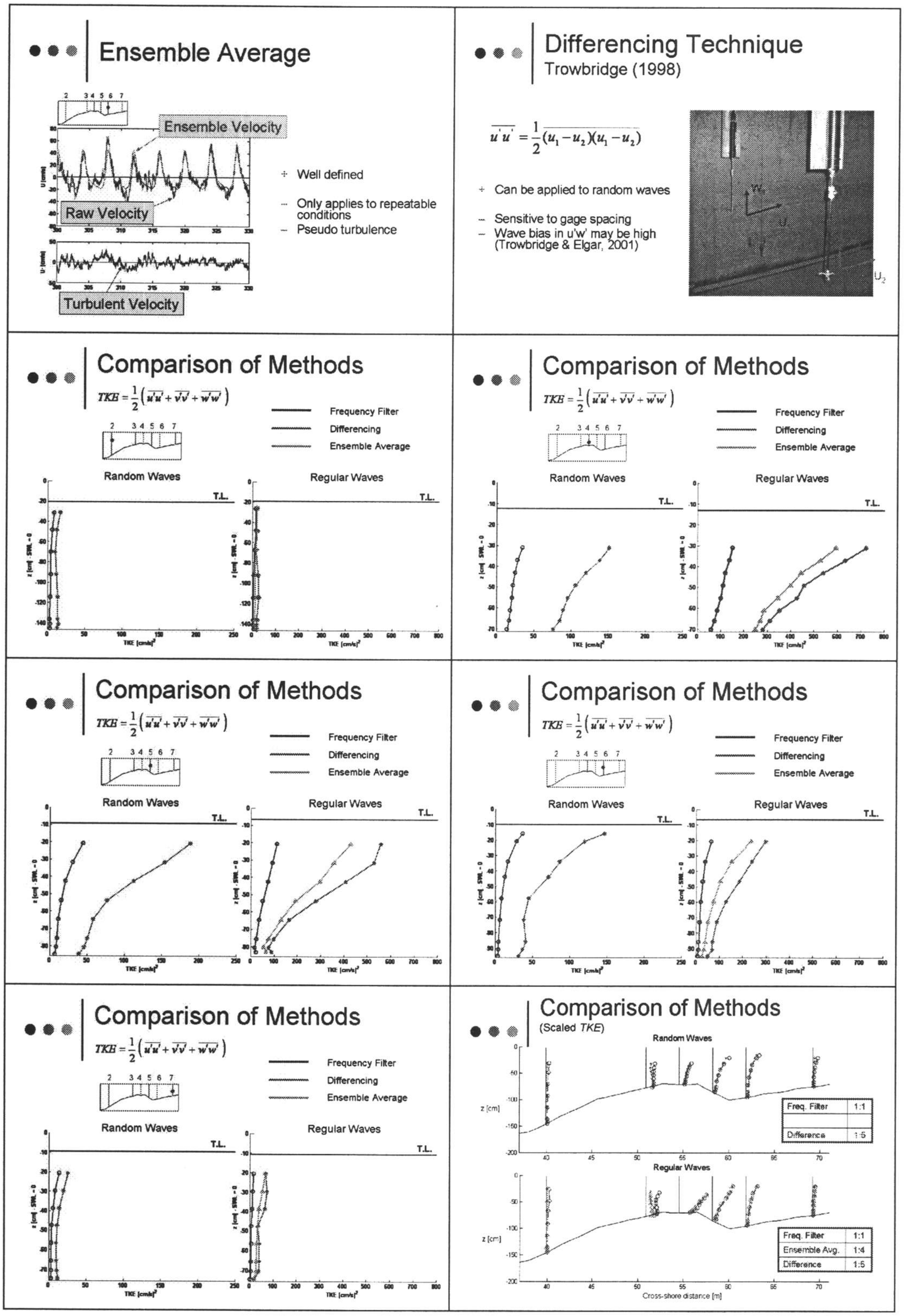

Figure F.3: Slides 17-24 presented at ICCE 2004. Organized left to right, top to bottom.

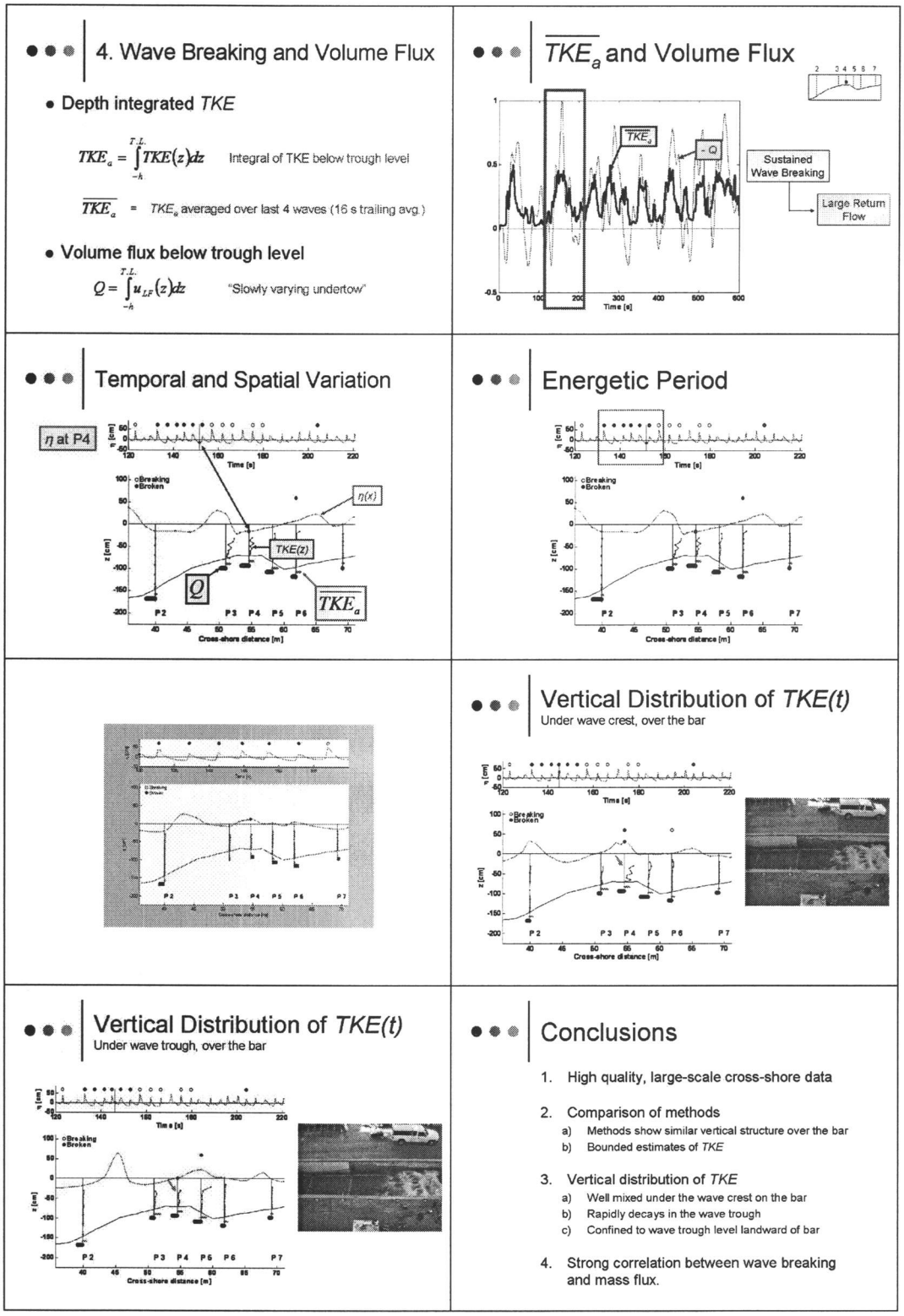

Figure F.4: Slides 25-32 presented at ICCE 2004. Organized left to right, top to bottom.

Appendix G. Poster Presented at Oceans/Techno-Ocean'04, Kobe, Japan

The work contained herein was also presented in a poster competition at the Oceans/Techno-Ocean'04 conference in Kobe, Japan on November 10-11, 2004. The Office of Naval Research (ONR) and National Defense Center of Excellence for Research in Ocean Sciences (CEROS) fund this program which provides students with the opportunity to experience an international conference and present their research by covering the cost of travel, lodging, and registration. Abstracts relating to coastal and ocean engineering were accepted from 43 students from the U.S. and abroad.

I attended the conference with Joe Long, another graduate student in the Ocean Engineering program at Oregon State University. Our posters were the only two focusing on coastal science and received less interest than some of the other posters on ocean engineering topics. However, the poster shown in Figure G.1 was awarded 3rd prize in the student competition. In addition to attending the conference, Joe and I were able to visit Takayuki Suzuki, who worked with us on this project, and Nobuhito Mori in Osaka, Japan. It was an excellent trip and I'd highly recommend that students search for opportunities such as this to present their research and experience other cultures.

SURF ZONE TURBULENCE ESTIMATES FROM A LARGE-SCALE LABORATORY FLUME

Christopher P. Scott (scottc2@engr.orst.edu), Daniel T. Cox, Timothy B. Maddux, Joseph W. Long, Emi E. Fujii

O.H. Hinsdale Wave Research Laboratory, Dept. of Civil, Const., and Env. Engineering, Oregon State University

http://wave.oregonstate.edu

Motivation & Objectives

State of Nearshore Processes Research II (Thornton, et al. 2000)

> *"Breaking waves, bottom boundary layers, and associated turbulence are important to wave energy dissipation and sediment transport, but are not understood well . . . and prototype-scale laboratory experiments can facilitate our efforts."*
>
> *"Wave and breaking-wave induced currents drive nearshore sediment transport, so understanding these flows is a prerequisite to predicting morphological change."*

In the laboratory, the fixed bed and repeatability of the incident wave conditions provide a unique opportunity to collect a detailed, synoptic data set of surf zone hydrodynamics. From this data set we can better understand the influence of wave breaking on the vertical and cross-shore structure of turbulence and the mean flow. This understanding is essential to improve predictions of morphological change.

Therefore, the present work outlines a laboratory experiment designed to:

1. Observe in detail the hydrodynamics of regular and random waves breaking on a barred beach.
2. Compare turbulent kinetic energy estimates from three methods used to separate wave-induced and turbulent components of fluid velocity.
3. Analyze the cross-shore and vertical structure of the turbulence generated by wave breaking.
4. Investigate the importance of wave breaking to mean flow characteristics.

Experimental Setup

WRL Large Wave Flume

- 104 m long, 3.7 m wide, 4.3 m deep
- Maximum wave height 1.6 m at period of 3.5 s
- Bathymetry approximates the bar geometry observed in the field at a 1:3 scale. (e.g., Oct. 11, Duck, NC 1994, [Garcez Faria 2000])

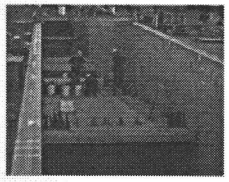

Figure 1. Installation of the model beach, looking offshore (toward the wavemaker).

Instrumentation and Test Conditions

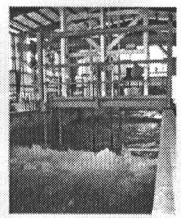

Figure 2. ADV array used to collect velocity profiles. Each profile contained measurements at 1 cm, 5 cm, and 10 cm above the fixed bed, and at 3 evenly-spaced locations up to trough level.

Table 1. Deep water and breaking wave conditions measured during the experiment.

	T	H_o	L_o	ξ	H_b	d_b	d_t	h_{mo}	R_{wave}
	[s]	[m]	[m]	[-]	[m]	[m]	[-]	[m]	[-]
Random	4.0	0.59	25.0	0.18	0.64	10.9	0.17	26	340
Periodic	4.0	0.64	25.0	0.17	0.75	10.9	0.16	16	150

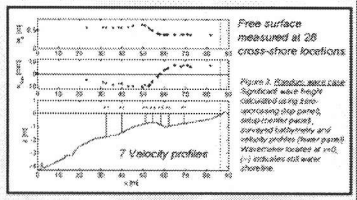

Figure 3. Random wave case. Significant wave height calculated using zero-upcrossing step paired, setup-corrected pressure, surveyed bathymetry and velocity profiles (lower panel). Wavemaker located at x=0, (+) indicates still water shoreline.

Comparison of Turbulence Separation Methods

To analyze turbulence in the coastal zone, the turbulent component of velocity must be separated from the wave-induced and mean flow components. This is a difficult process and several methods exist to do so. Here, three methods are compared:

- *frequency filtering (1 Hz cutoff) – e.g., Nadaoka and Kondoh 1982*
- *ensemble averaging – e.g., Ting and Kirby 1994*
- *differencing – Trowbridge 1998*

This extends the work of Svendsen (1987) by directly comparing the time-averaged estimates of the turbulent kinetic energy, k, obtained using each of the three methods. This allows others to interpret experimental results obtained using different techniques.

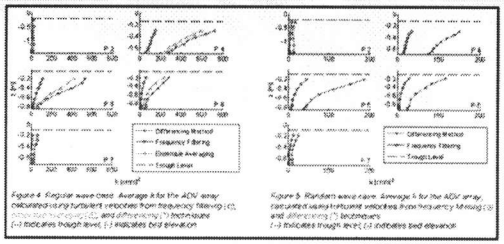

Figure 4. Regular wave case. Average k for the ADV array, calculated using turbulent velocities from frequency filtering (□), ensemble averaging (○), and differencing (▽) techniques. (–) indicates trough level, (-) indicates bed elevation.

Figure 5. Random wave case. Average k for the ADV array, calculated using turbulent velocities from frequency filtering (□) and differencing (▽) techniques. (–) indicates trough level, (-) indicates bed elevation.

Figure 4 and Figure 5 show that the frequency filter always provides a low estimate of k, which is most likely due to the energy neglected from large eddies with frequencies lower than 1 Hz, and is consistent with the observations of Svendsen (1987). Figure 4 also shows that the differencing technique estimates k to within 25% of values derived from ensemble averaging. Therefore, the differencing technique should estimate k fairly well for random wave conditions.

The shape of the vertical profile of k seems to be independent of the method used to extract the turbulent signal at each profile. To investigate this possibility, the estimates obtained from each method were scaled as shown in Table 2.

Table 2. Scaling used to show that a simple relationship exists between each method.

Frequency Filtering	Ensemble Averaging	Differencing
1.0	1.0	1.0

A comparison of k, scaled using Table 2, (Figure 6) indicates that a simple scaling (same value used at all cross-shore and vertical locations) does exist as each of the estimates collapse onto a single profile at each location for both random and regular wave fields.

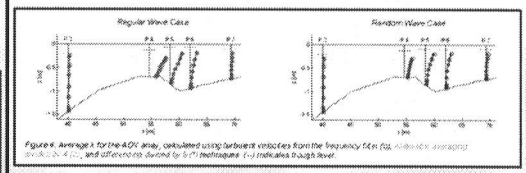

Figure 6. Average k for the ADV array, calculated using turbulent velocities from the frequency filter (□), ensemble averaging (○), and differencing (▽) techniques (–) indicates trough level.

From Figure 6 it is clear that the turbulent intensity is largest over the bar and does not completely dissipate prior to reaching the bed. This suggests that the turbulence generated by wave breaking is important for near-bed processes such as sediment suspension and transport. This also appears to be a feature localized to the bar crest, as only a few meters onshore (P5) k is confined to the upper portion of the water column, a trend that continues shoreward (P6). Within approximately 1.5 wavelengths of the bar crest (P7) there is little turbulence within the water column, consistent with visual observations of reformed waves at this location.

Wave Breaking and Mass Flux

Observations of the low frequency fluctuation of the velocity indicated that there existed a correlation between periods of intense breaking and a strong offshore-directed flow during the random wave case. To study this in more detail, the depth integrated turbulent kinetic energy, k_{int}, provided a good indicator for the intensity of wave breaking. This was then averaged using a trailing average over 4 waves, 16 s, to allow time for the mass introduced by breaking to return offshore (k_{lp}).

The mass flux, Q, was then calculated by integrating the low-frequency component of the cross-shore velocity (u_{LF}), the "slowly varying undertow," to trough level. This slowly varying undertow was calculated by low-pass filtering the u component of velocity using a cutoff frequency of 0.0625 Hz, 1/4 of the wave peak frequency.

Figure 7 illustrates the correlation between k_{lp} and Q at a location directly over the bar crest (P4). Note that in this figure $-Q$ is plotted such that a positive value indicates an offshore-directed flux, and k_{lp} and Q are normalized by $2(k_{lp})_{max}$ and Q_{max}, respectively, for plotting. This figure indicates that the wave breaking process is not only important in terms of the turbulent velocities and their interaction with sediment, but also in terms of forcing changes in the mean flow magnitude and direction. Further work is needed to relate these quantities to the variation in the setup over the bar.

$$k_{int}(t) = \int_h^{\eta} k(z,t)\,dz$$

$$k_{lp}(t_i) = \frac{\Delta t}{\Delta T} \sum_{t=t_i-\frac{\Delta T}{2}}^{t_i+\frac{\Delta T}{2}} k_{int}(t)$$

$$Q(t) = \int_h^{\eta} u_{LF}(z,t)\,dz$$

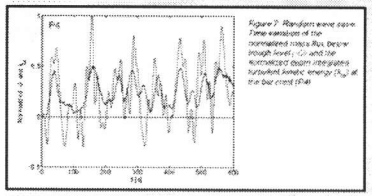

Figure 7. Random wave case. Time variation of the normalized mass flux, $-Q$, (trough level), (○) and the normalized depth integrated turbulent kinetic energy (k_{lp}) at the bar crest (P4).

Conclusions

One of the first large-scale, synoptic data sets to study the wave breaking process on a barred beach for random and regular waves has been collected.

A comparison of 3 methods to separate the wave-induced and turbulent components of velocity shows:

- The differencing method proposed by Trowbridge (1998) produces estimates of the turbulent kinetic energy within 25% of those obtained by ensemble averaging.
- Using a simple scaling, the shape of the vertical profile of k was found to be independent of the method used to extract the turbulence.

Study of the wave breaking hydrodynamics shows:

- The turbulent intensity is largest at the bar crest, where it penetrates to the bottom, but is quickly confined to the upper layer landward of the bar, and effectively dissipated within 1.5 wavelengths of the bar crest.
- Observed correlation between the depth integrated turbulent kinetic energy and the mass flux to trough level indicates that wave breaking is important in forcing the mean flow averaged over a few wave periods.

This data set will also be used to guide the development of numerical models designed to predict nearshore hydrodynamics and sediment transport.

Acknowledgements

This work was partially funded by the National Science Foundation under grants No. CMS-0086571, EEC-0244205 and OCE-0351741. The success of this project was due to the contributions of many, especially Terry Dibble at the WRL.

References

Garcez Faria, A.F.G., E.B. Thornton, T.C. Lippmann, and T.P. Stanton, 2000. Undertow over a barred beach, J. Geophys. Res., 105(C7), 16999-17010.

Nadaoka, K., and T. Hondoh, 1982. Laboratory measurements of velocity field structure in the surf zone by LDV, Coastal Eng. in Japan, 25, 125-145.

Svendsen, I.A., 1987. Analysis of surf zone turbulence, J. Geophys. Res., 92(C5), 5115-5124.

Thornton, E.B., R.A. Dalrymple, T. Drake, E. Gallagher, R.T. Guza, A. Hay, R.A. Holman, J. Kaihatu, T.C. Lippmann, and T. Cuban-Haller, 2000. State of nearshore processes research, II, Technical Report NPS-OC-00-001, Naval Postgraduate School, Monterey, CA, 97 pp.

Ting, F.C.K., and J.T. Kirby, 1994. Observation of undertow and turbulence in a laboratory surf zone, Coastal Eng., 24, 51-80.

Trowbridge, J., 1998. On a technique for measurement of turbulent shear stress in the presence of surface waves, J. Atmos. Oceanic Technol., 15, 290-298.

Figure G.1. Poster presented at Oceans/Techno-Ocean'04, Kobe, Japan